UPPER BOUND ANALYSIS OF BEARING AND OVERTURNING CAPACITIES OF SHALLOW FOUNDATIONS IN SOFT CLAY

A Thesis

by

RANDAL JAMES HARTSFIELD

Submitted to the Office of Graduate and Professional Studies of
Texas A&M University
in partial fulfillment of the requirements for the degree of

MASTER OF SCIENCE

Chair of Committee,	Charles Aubeny
Committee Members,	Giovanna Biscontin
	Jerome Schubert
Head of Department,	Yunlong Zhang

December 2013

Major Subject: Civil Engineering

ABSTRACT

This thesis presents a method to calculate the bearing and overturning capacity of a shallow foundation installed in soft clay using the upper bound method of plasticity. Mudmats are commonly used shallow foundations in offshore projects and are often eccentrically loaded. As economics and project requirements change, mudmats have evolved from simple circles and rectangles to more complex geometries. Computing the bearing and overturning capacities of such complex geometries using existing methods outlined in API procedures becomes difficult, as these procedures have been established for simple shapes. FEM is an alternative and established method for analysis, but these programs can be costly.

In this thesis, the procedures for analysis using the upper bound method of plasticity are outlined and used to compute the bearing and overturning interaction for several foundations of varying shapes and undrained shear strength profiles. These results are compared to output of the FEM analysis program ABAQUS for validation.

The conclusions of this case study are that the upper bound method of plasticity provides a reasonable prediction of the bearing and overturning capacity of an eccentrically loaded mudmat foundation, though considerations should be made when significant torsion or overturning moments in multiple directions are expected.

NOMENCLATURE

A	Area of foundation
A'	Effective area of foundation
B	Width of foundation
B'	Effective width of foundation
c	Undrained shear strength
D	Depth of embedment
$\dot{D}$	Dissipation rate
e_1	Eccentricity along axis-1
e_2	Eccentricity along axis-2
$\dot{E}$	Work rate due to eccentric load
F	Footing correction factor as a function of $\frac{\kappa \cdot B'}{s_{u0}}$
F_v	Vertical force applied to foundation
$f(Q, M)$	Interaction surface
i	Subscript representing element number
K_c	Footing correction factor accounting for load inclination, footing shape, depth of embedment, inclination of base, and inclination of seafloor surface
L'	Effective length of foundation
L_1	Planar dimension of foundation along axis-1

L_1'	Effective planar dimension of foundation along axis-1
L_2	Planar dimension of foundation along axis-2
L_2'	Effective planar dimension of foundation along axis-2
L_x	Planar dimension of foundation along axis-x
M	Moment applied to foundation
M_1	Moment applied to foundation about axis-1
M_2	Moment applied to foundation about axis-2
n	Total number of elements in foundation
N_c	Bearing capacity constant equal to $2 + \pi$
N_m	Overturning capacity constant equal to $\frac{\pi}{4}$
Q	Bearing capacity of foundation, or foundation element
Q_0	Bearing capacity of foundation, or foundation element, as calculated from one of the prescribed methods
s_u	Undrained shear strength
s_{u0}	Undrained shear strength at the foundation base level
x	Location of centroid of foundation element along axis-x
x_0	Location of axis of rotation along axis-x
x_e	Location of applied eccentric load along axis-x
$\dot{\beta}$	Virtual rate of rotation
γ	Total unit weight of the soil, unit weight
$\dot{\delta_v}$	Virtual rate of displacement

$\dot{\theta}$	Virtual rate of rotation
κ	Rate of linearly increasing undrained shear strength with depth

TABLE OF CONTENTS

LIST OF FIGURES

LIST OF TABLES

INTRODUCTION

Mudmat foundations are popular shallow foundations used in offshore projects. An example mudmat foundation is shown in Figure 1, which is awaiting install.

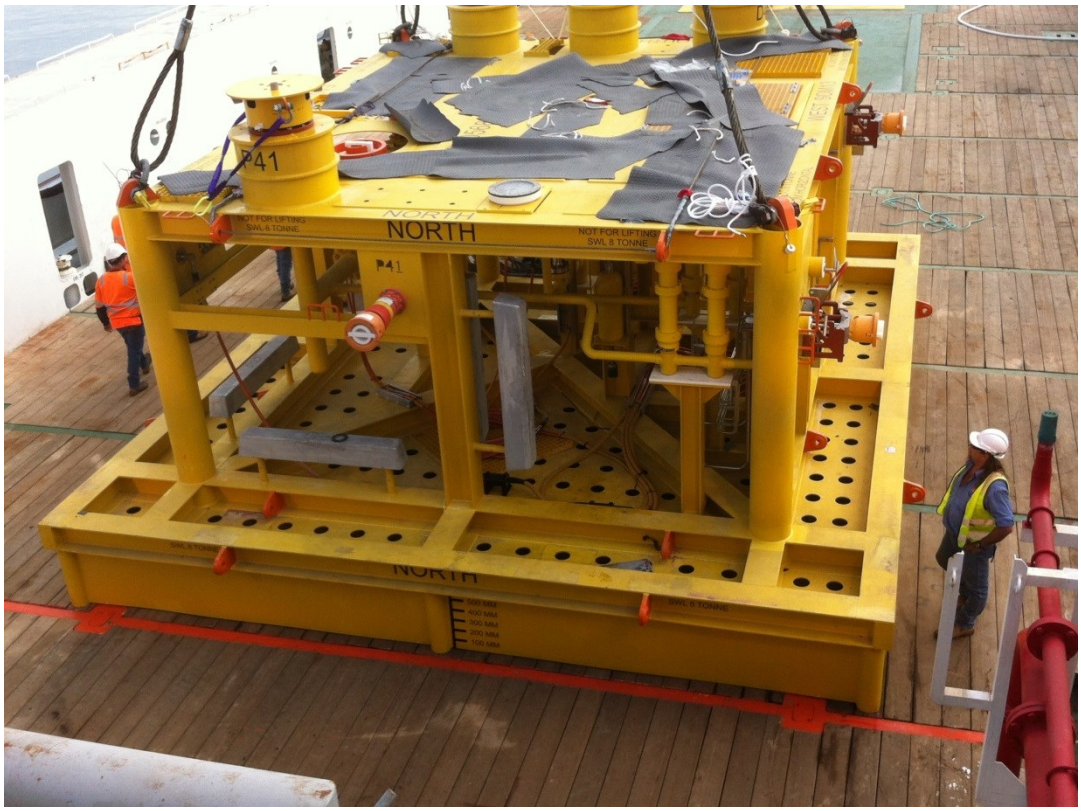

Figure 1. Mudmat foundation before installation (courtesy of confidential client)

Mudmats range in size and complexity of the bearing surface to adequately resist design loading conditions. Figure 2 shows a mudmat foundation with two footings which are connected by the supported structure in order to resist overturning moments in one direction.

Figure 2. Mudmat foundation with two footings (Randolph et al, 2010)

There is extensive literature discussing methodologies for assessing the bearing capacity of mudmat foundations for the offshore environment. These methodologies attempt to address design challenges such as:

- Eccentric loading due to overturning moments
- Variability in soil shear strength profile with depth
- Effects of shape of the foundation, depth of embedment, and ground slope

The American Petroleum Institute (API) has established methods for bearing and overturning capacity analysis that address these design challenges after previously published methods (such as Vesic, 1975 or Davis and Booker, 1973). These are included in:

- API RP 2A (American Petroleum Institute, 2005)
- API RP 2GEO (American Petroleum Institute, 2011)

Finite element methods (programs such as ABAQUS, PLAXIS, etc.) are also used for geotechnical mudmat analyses.

In the United States, the current state of the practice for designing mudmat foundations in undrained soils is to use the methods outlined in API Recommended Practices for constant and linearly increasing undrained shear strength profiles. When design constraints restrict the use of these methods, finite element methods (FEM) or other alternative methods are recommended (American Petroleum Institute, 2011).

LOADING CONDITIONS

Mudmat foundations are typically subject to loads in six degrees of freedom. This includes vertical and lateral forces, and torsion and overturning moments. We refer to overturning moments as "eccentric loads," as they can be modeled as a vertical force

applied at a distance from the centroid equal to the applied moment divided by the applied vertical force. These eccentric loads reduce the bearing capacity of the foundation, and are addressed in methods outlined in API codes.

ISSUES IN DESIGN – COMPLEX GEOMETRIES

The shape of a mudmat foundation may vary considerably to adapt to the needs of different offshore projects. Simple square and rectangular shapes are the most popular, although A-frames, H-frames, and rectangular shapes with center cut-outs are not uncommon. Sample mudmat geometries are shown in Figure 3 and Figure 4. It becomes increasingly difficult to analyze mudmat foundations of these complex geometries using design codes from API.

Finite element methods are typically employed to predict the bearing capacity for irregular shapes, as previously described. FEM may also model variations in shear strength with depth and eccentric loading to the foundation.

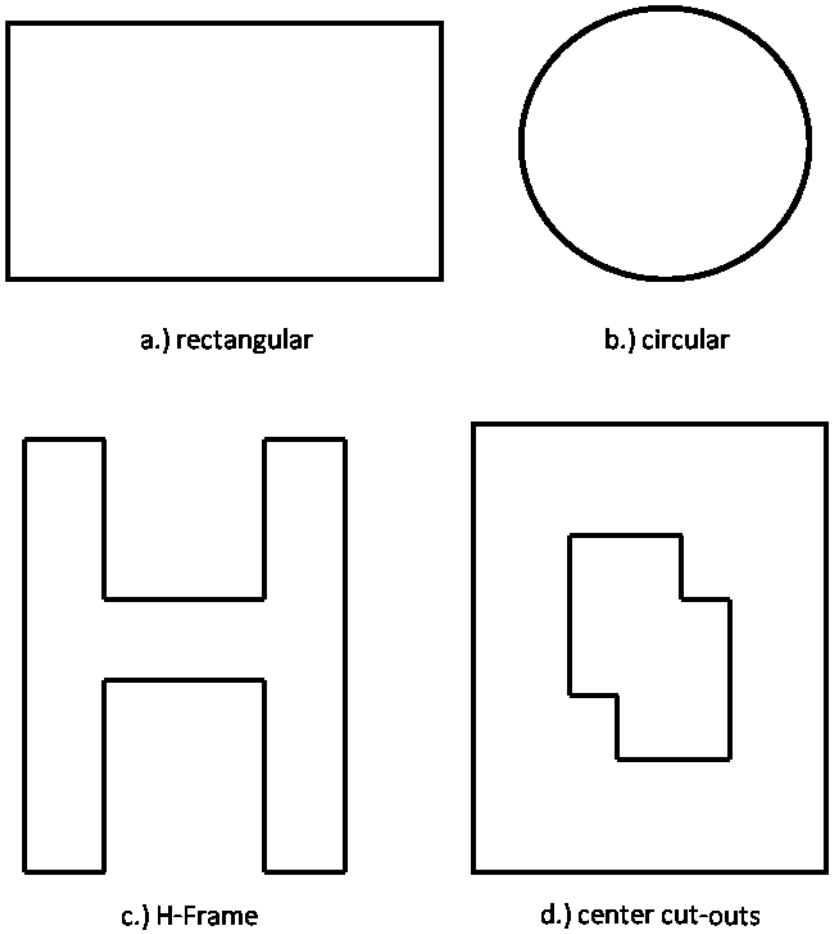

Figure 3. Example mudmat geometries

Figure 4. Complex footing pads at each corner of structure (fibregate.co.uk)

The bearing capacity of a mudmat foundation under eccentric loading can also be predicted using 2-D upper bound plasticity solutions, which will be the focus of this thesis. This procedure is not widely used in design, especially for simple rectangular and square foundation shapes. However, upper bound plasticity solutions can be a useful tool when analyzing the bearing capacity of irregular shapes.

OBJECTIVES

The objectives of this thesis are to:

- Present a new method for calculating the bearing capacity of a mudmat foundation that addresses the challenge of complex geometries
- Validate this method through FEM

The following sections describe the limitations of established bearing and overturning capacity methods and present a new method based on the upper bound plasticity approach. This thesis considers a mudmat foundation on two different undrained shear strength profiles. The bearing capacity for each soil profile is calculated using upper bound plasticity solutions and shows proof of concept through comparison with FEM analyses using ABAQUS.

BACKGROUND

There are several methods for calculating the bearing capacity of the shallow foundation depending on soil type, soil strength profile, and foundation shape. The following sections describe recommended practices from API (after methods proposed by Vesic (1975) and Davis and Booker (1973)) that have been widely accepted in the United States and used for offshore mudmat design in undrained soils.

API RP 2A: CONSTANT UNDRAINED SHEAR STRENGTH PROFILES

API RP 2A (American Petroleum Institute, 2010) gives general guidelines for the analysis of offshore structures. Specific guidance is given for the undrained bearing capacity of shallow foundations for a constant undrained shear strength profile.

In API RP 2A, the undrained bearing capacity is defined as:

$$Q = (cN_cK_c + \gamma D)A' \qquad \text{Equation (1)}$$

Equation (1) is the extended form of the bearing capacity equation presented by Hansen (1970) and Vesic (1975). The dimensionless correction factor, K_c, representing the product of individual factors accounting for load inclination, shape, depth of embedment, base inclination, and ground inclination (Vesic, 1975). This equation agrees well with failure conditions observed in large scale studies conducted by Meyerhof (1963).

This method of analysis is strictly applicable to a constant undrained shear strength profile, although reasonable assessments of equivalent uniform properties is allowed (American Petroleum Institute, 2010).

API (2010) acknowledges limitations and special considerations should be made when:

- Undrained shear strength is highly variable over the depth of influence, or is highly anisotropic
- Loading conditions deviate from simplified assumptions, such as the presence of a high torsional moment
- Loading rates do not clearly define drained or undrained soil response
- Foundation shapes are highly irregular

Among several alternative approaches, API suggests the use of limit equilibrium methods (Murff and Miller, 1977-1) and numerical analyses (such as FEM).

API RP 2GEO: LINEARLY INCREASING UNDRAINED SHEAR STRENGTH PROFILES

API RP 2GEO (American Petroleum Institute, 2011) outlines geotechnical design considerations for offshore structures. Specific guidance is given for the undrained bearing capacity of shallow foundations for two undrained shear strength profiles: constant shear strength with depth and idealized linearly increasing shear strength with depth. This section focuses on an undrained shear strength profile that linearly increases with depth (a common profile at offshore sites).

Davis and Booker (1973) studied the effects of increasing undrained shear strength on the bearing capacity of shallow foundations. They discovered that the rate of increasing shear strength with depth plays the same role as density in the bearing capacity of homogeneous, cohesive-frictional soils (Davis and Booker, 1973).

For a linearly increasing undrained shear strength profile, API RP 2GEO recommends the undrained bearing capacity be calculated after the method proposed by Davis and Booker (1973):

$$Q = F\left(s_{u0}N_c + \frac{\kappa B'}{4}\right)K_c A' \qquad \text{Equation (2)}$$

The dimensionless correction factor, K_c, for this equation is the sum of individual factors accounting for load inclination, shape, depth of embedment, base inclination, and ground inclination.

For this method, the value of s_{u0} is taken to be the undrained shear strength at the base of the foundation and the value of κ is taken to be the linear rate of strength increase with depth from the base of the foundation. This is illustrated in Figure 5.

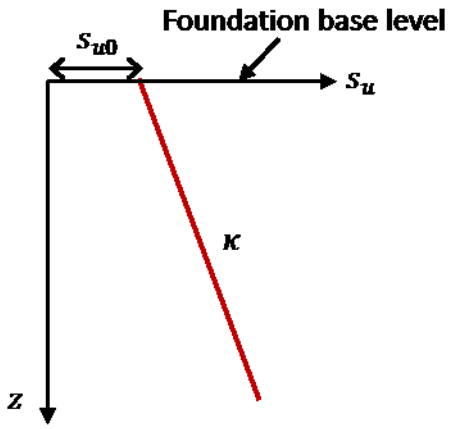

Figure 5. Undrained strength parameters for Davis and Booker (1973) analysis

It should be noted that Davis and Booker (1973) derived Equation (2) through the application of plasticity theory, which is described in the following section of this thesis.

This method is also limited to simple foundation geometries and loading conditions. As with API RP 2A, API RP 2GEO suggests using alternative methods and/or design approaches to verify the results as appropriate (American Petroleum Institute, 2011).

EFFECTS OF SHAPE ON THE BEARING CAPACITY FACTOR

In undrained soils, the bearing capacity factor, N_c, is multiplied by the undrained strength to model the bearing failure mechanism and is a function of the shape of the foundation. N_c is equal to $2 + \pi$ (5.14) for a strip footing and will increase up to 6.14 for a square or circular footing when multiplied by a correction factor for the shape of the footing, s_c. The variation of N_c with foundation shape is shown in Figure 6.

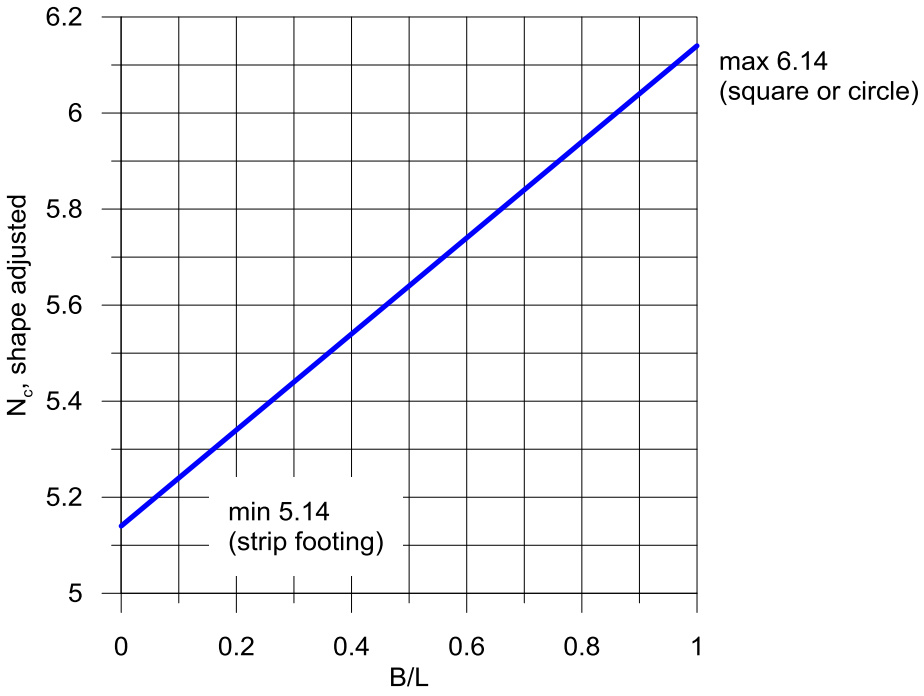

Figure 6. Bearing capacity factor adjusted for shape

In the two previously described bearing capacity calculation methods, the value of N_c is equal to 5.14 regardless of shape. The effects of shape are considered in the correction factor, K_c. As the ratio of the length to the width of the foundation decreases (i.e. the foundation behaves less like an infinite strip footing and more like a square or circular footing) the value of K_c will generally increase to modify the bearing capacity factor. However, the correction factor is also a function of other foundation conditions, such as load inclination, base and ground inclination, and depth of embedment. Therefore, the correction factor may still be less than 1.0 if high load inclinations or base and ground inclinations are expected.

EFFECTS OF OVERTURNING ON THE BEARING FACTOR

For the condition of pure bearing, the bearing capacity factor, N_c, for a strip footing on soil with a constant undrained shear strength profile can be estimated from rearranging the classical bearing capacity equation for undrained soils:

$$N_c = \frac{Q}{s_u \cdot A} = 2 + \pi \qquad \text{Equation (3)}$$

The pure overturning capacity can be estimated from rearranging the moment equilibrium equation, assuming a semi-circular slip surface, and calculating the shear resistance along the failure plane:

$$M = s_u \cdot \left(\pi \cdot \frac{B}{2}\right) \cdot \frac{B}{2} \cdot L \qquad \text{Equation (4)}$$

We compute the moment capacity factor, N_m, through rearranging Equation (4):

$$N_m = \frac{M}{s_u \cdot A \cdot B} = \frac{\pi}{4} \qquad \text{Equation (5)}$$

The bearing capacity factor for a foundation element in pure overturning is equal to π.

Eccentric loading is common for offshore shallow foundations. The failure mechanism for such loading includes vertical displacements and rotations. This affects the bearing pressure beneath the foundation, as foundation elements near the axis of rotation will tend to be in pure rotation and the elements away from the axis of rotation will be nearer to pure bearing.

We will consider an element to be in pure bearing when it is at a distance of $\frac{B}{2}$ from the axis of rotation, and approximate the bearing factor for intermediate elements as a linear relationship between π and $2 + \pi$ (Figure 7).

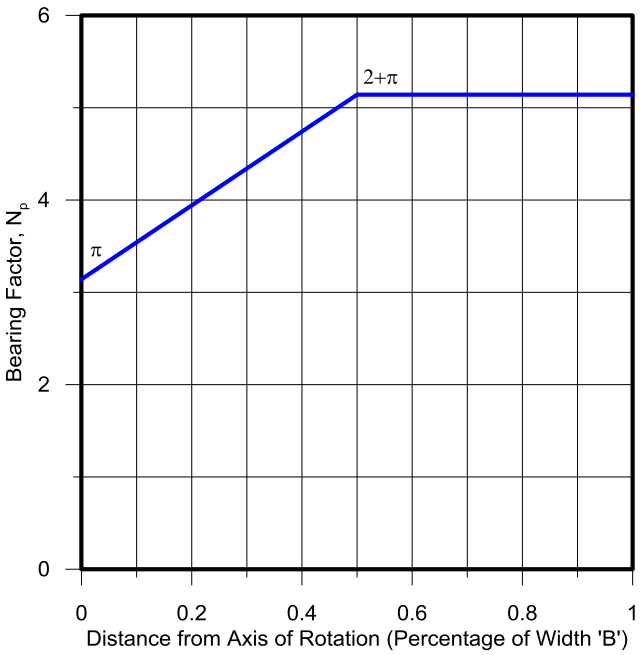

Figure 7. Variation of the bearing factor with distance from axis of rotation

EFFECTS OF ECCENTRIC LOADING

Model tests conducted by Meyerhof (1963) and Hansen (1970) indicate that the foundation bearing area under eccentric loading is reduced to an "effective" bearing area. This reduction in bearing area in turn decreases the ultimate bearing capacity of the structure.

API (2010, 2011) has adopted the effective bearing area approach when analyzing the bearing capacity with respect to eccentric loads. This method reduces the planar dimensions of the foundation due to eccentricities in both planar directions from overturning moments. The effective dimensions are defined as (American Petroleum Institute, 2010 and American Petroleum Institute, 2011):

$$L_1' = L_1 - 2e_1 = L_1 - 2\frac{M_2}{F_v} \qquad \text{Equation (6)}$$

$$L_2' = L_2 - 2e_2 = L_2 - 2\frac{M_1}{F_v} \qquad \text{Equation (7)}$$

The shortest of the two dimensions, L_1' and L_2', is considered the effective width, B', and the longer of the two dimensions is considered the effective length, L'. The product of these effective dimensions is the effective area, A' (Figure 8).

Oftentimes, resultant eccentric loads applied to mudmat foundations are due to lateral forces applied to the foundation. These lateral forces will decrease the bearing and overturning capacity of the foundation (American Petroleum Institute, 2010, 2011). Therefore, adjustments should be made to the bearing factor based on the shear demand due to sliding. For this calculation, we can relate the bearing factor to the shear demand due to sliding through Equation (8).

$$\left(\frac{N_p}{N_{pmax}}\right)^2 + \left(\frac{N_s}{N_{smax}}\right)^2 = \left(\frac{N_p}{N_{pmax}}\right)^2 + \left(\frac{H}{s_u \cdot A \cdot \alpha}\right)^2 = 1 \qquad \text{Equation (8)}$$

Equation (8) is a simplification of existing methods of reducing the bearing and overturning capacity due to lateral loading, often termed “inclined loading.” API has

similar reductions in API RP 2A (American Petroleum Institute, 2010) and API RP 2GEO (American Petroleum Institute, 2011).

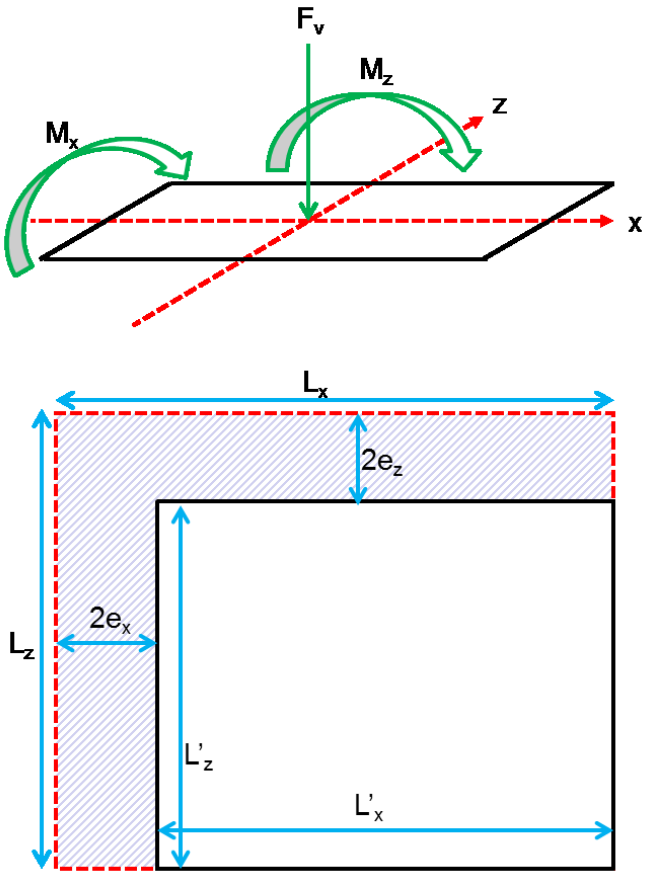

Figure 8. Effective mudmat dimensions

PLASTIC LIMIT ANALYSIS

Plastic limit analysis is used to predict the load carrying capacity of structures composed of rate-independent, ductile materials. This method ignores elastic deformation and instead focuses on the strength of the system, assuming small plastic deformation (Murff, 2008).

This section gives some background on plastic limit analysis in geotechnical engineering and describes the application of the upper bound approach in predicting the bearing capacity of an eccentrically loaded shallow foundation.

Background

The theory of plasticity makes the following assumptions (Chen and Liu, 1991):

- The material is rigidly perfectly plastic (no strain hardening or work softening, and deformation beyond the yield point is insignificant)
- Tresca or von Mises yield criterion
- The material follows the associated flow rule (the strain increment direction is normal to the yield surface)

We can apply the theory of plasticity through the principle of virtual work (Chen and Liu, 1991). This principle assumes a virtual rotation rate and/or virtual displacement rate in order to calculate the work rate of the system. Calculating the virtual work done by each force in a body and setting this equal to zero is akin to writing the equilibrium equations in the direction of movement (Calladine, 1969).

Rigid, Perfect Plasticity

Soft, undrained soils display nonlinear behavior during loading. When these soils undergo very small strains, the stress-strain curve is very nearly linear. For simplicity, we choose to model the initial part of the stress-strain curve as linear. As the soil deforms to and beyond the undrained strength, the shear stress decreases to a residual strength by a process known as work softening. This portion of the curve represents the plastic behavior of the soil, since the shear stress will remain relatively constant with continued deformation. Figure 9 shows this relationship (plotted in blue).

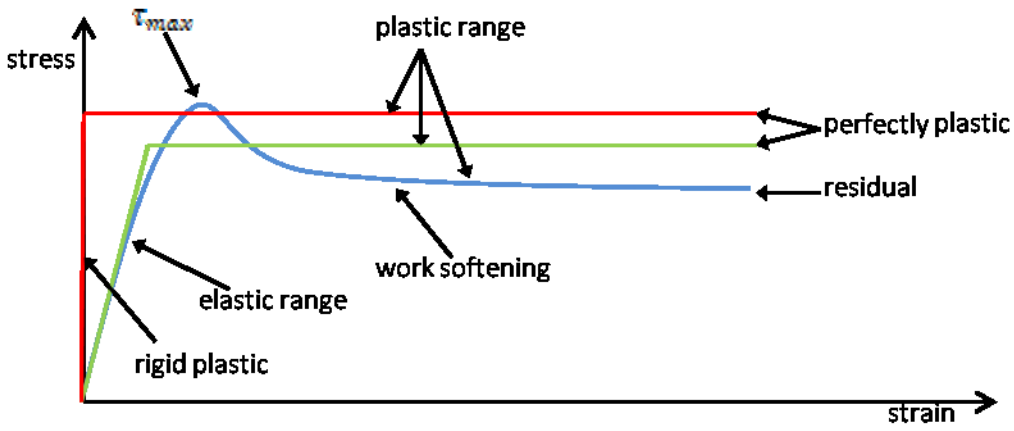

Figure 9. Stress-strain for elasto-plastic and perfectly plastic soils

We can idealize soil as perfectly plastic by neglecting work softening because we are interested in capacity, not displacement. Figure 9 shows an idealized perfectly

plastic stress-strain relationship, along with an elastic modulus representing the elastic behavior of the soil during initial deformation (plotted in green).

Plasticity theory assumes a perfectly plastic model that is rigid, meaning the soil does not experience elastic deformation. Thus, deformation will only occur when the shear stress in the soil reaches its peak value, similarly to the way a mass at rest on the ground may only translate when the frictional resistance is overcome. An idealized rigid, perfectly plastic relationship is included in Figure 9 (plotted in red).

Yield Criterion

The yield surface represents the boundary between the possible and impossible states of stress in a body. All possible states of stress (in combinations of major and minor principal stresses) are located inside the yield surface. For a rigid, perfectly plastic material, there is no deformation within the yield surface. The impossible states of stress (or where deformation occurs in a rigid, perfectly plastic material) are located outside the yield surface.

The most common yield criterion in undrained soils is the Tresca criterion (Murff, 2008), which can be expressed in terms of the major and minor principal stresses as:

$$\frac{\sigma_1 - \sigma_3}{2} = \tau_{max} = s_u \qquad \text{Equation (9)}$$

Other stresses are assumed to have no effect on yielding.

The von Mises criterion assumes all terms causing shear stress will affect yielding (Murff, 2008), and is expressed as:

$$\left[\frac{1}{6}\left[\left(\sigma_x-\sigma_y\right)^2+\left(\sigma_y-\sigma_z\right)^2+\left(\sigma_z-\sigma_x\right)^2\right]+\tau_{xy}^2+\tau_{yz}^2+\tau_{zx}^2\right]^{1/2}=\tau_{max}=k \qquad \text{Equation (10)}$$

We can compare the two yield surfaces by considering a simple unconfined, undrained (UU) triaxial compression test ($\sigma_2=\sigma_3$). In this case, Equation (10) reduces to:

$$\frac{\sigma_1-\sigma_3}{\sqrt{3}}=\tau_{max} \qquad \text{Equation (11)}$$

Thus, τ_{max} is about 15.5 % greater for von Mises criterion than for Tresca criterion for UU triaxial compression tests.

Which criterion is used is often based on mathematical convenience, since the scatter in strength measurements may obscure small differences in τ_{max} for both criteria (Murff, 2008). The Tresca yield criterion is typically used to model undrained behavior in 2-D plasticity analyses, while the von Mises criterion is simpler to use for 3-D analyses (Murff and Miller, 1977-2 and Murff, 2008). Plots of the Tresca and von Mises criteria are shown in Figure 10.

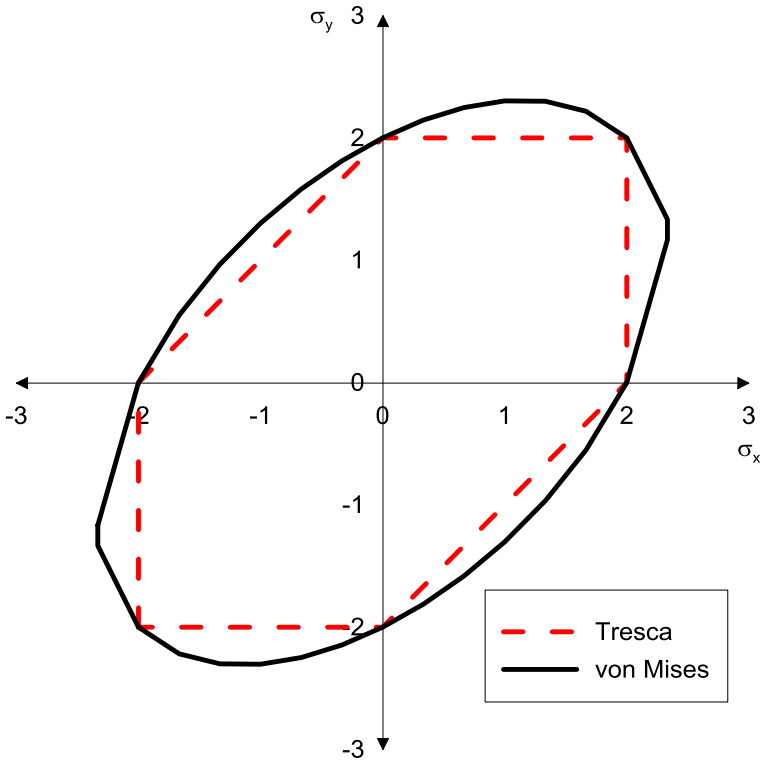

Figure 10. Tresca and von Mises yield surfaces

Associated Flow and Normality

The stresses required to bring the soil to the yield surface will also dictate the strain direction once the stress state reaches yield. If we consider rigid, perfectly plastic soil response, the potential function (a vector which defines the magnitudes and directions of the strains for a given stress state) will be equal to the yield function. When the potential function is equal to the yield function, it is described as "associated flow." This means that the strain direction will be a vector that is normal to the yield surface, as shown in Figure 11 (Murff, 2008 and Kim, 2005).

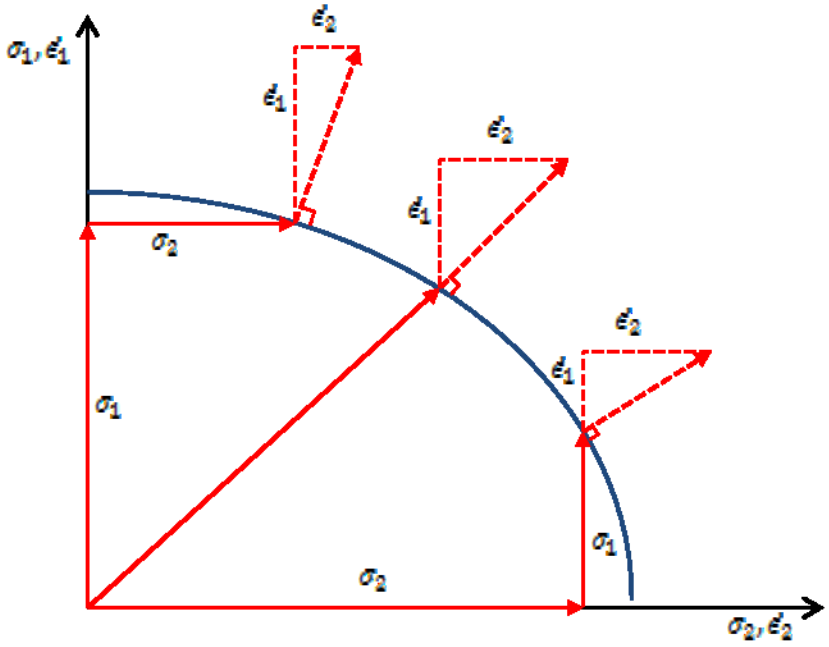

Figure 11. Associated flow rule and normality condition (Murff, 2008)

Bound Theorems of Plasticity

The theory of plasticity can be expressed in terms of the "bound theorems," which refer to the upper bound and lower bound methods of plasticity (Murff, 2008). In the lower bound method, we assume a stress field that satisfies equilibrium and is below the yield point everywhere in the structure. In the upper bound theorem, we assume a failure mechanism at which the stress field is at the yield point (Calladine, 1969). This thesis focuses on using the upper bound method of plasticity and its use in analyzing the response of eccentrically loaded shallow foundations.

Upper Bound Method

Calladine (1969) describes the upper bound theorem this way: "If an estimate of the plastic collapse load of a body is made by equating internal rate of dissipation of energy to the rate at which external forces do work in any postulated mechanism of deformation of the body, the estimate will be either high or correct."

In the upper bound method of plasticity, the work rate from applied loads is set equal to the internal energy dissipation rate along an assumed failure surface (Drucker and Prager, 1952). The unknown forces are evaluated and minimized to give an exact solution.

Murff (2008) gives the internal energy dissipation rate for a plastic material as:

$$\dot{D} = \sigma_i \dot{\epsilon}_i \qquad \text{Equation (12)}$$

The strain rate is equal to the partial derivative of the yield surface with respect to the applied stress multiplied by a scaling factor.

The upper bound method gives a solution through the virtual work method in the following steps (Murff and Miller, 1977-1):

- Define a kinematically admissible failure mechanism (with velocity field)
- Solve for the dissipation rate as a function of strain rate (preferably in terms of the strain rate in a single direction for 2-D problems)
- Equate the internal energy dissipation rate in the system to the work rate applied to the system by an unknown force

- Minimize the unknown force with respect to the length of the failure mechanism

To find the internal energy dissipation rate in the system, we need to define the strain rates in each direction. The equation for the yield function is the same regardless of Tresca or von Mises yield criterion (Murff, 2008 and Kim, 2005):

$$f(\sigma_{ij}) = \left[\left(\frac{\sigma_x - \sigma_y}{2}\right)^2 + \frac{1}{2}{\tau_{xy}}^2 + \frac{1}{2}{\tau_{yx}}^2\right]^{1/2} - s_u = 0 \qquad \text{Equation (13)}$$

We can apply the associated flow rule and take the partial derivative of the yield function with respect to each stress to obtain the strain rates in each direction, which are (in reduced form):

$$\dot{\varepsilon_x} = \lambda\frac{\partial f(\sigma_{ij})}{\partial \sigma_x} = \lambda\frac{\sigma_x - \sigma_y}{4 \cdot s_u} \qquad \text{Equation (14)}$$

$$\dot{\varepsilon_y} = \lambda\frac{\partial f(\sigma_{ij})}{\partial \sigma_y} = -\lambda\frac{\sigma_x - \sigma_y}{4 \cdot s_u} \qquad \text{Equation (15)}$$

$$\dot{\gamma_{xy}} = \lambda\frac{\partial f(\sigma_{ij})}{\partial \tau_{xy}} = -\lambda\frac{\tau_{xy}}{2 \cdot s_u} \qquad \text{Equation (16)}$$

In undrained conditions soil is incompressible, therefore the volumetric strain is subject to the constraint:

$$\dot{\varepsilon_v} = \dot{\varepsilon_x} + \dot{\varepsilon_y} = 0 \qquad \text{Equation (17)}$$

We commonly assume deformation occurs along a slip surface, which can be idealized as two rigid blocks (of unit dimensions) with a deformation zone of thickness t between them (Figure 12, after Murff 2008). In this model, one block is considered to be stationary and the other moves with relative velocity, v_0.

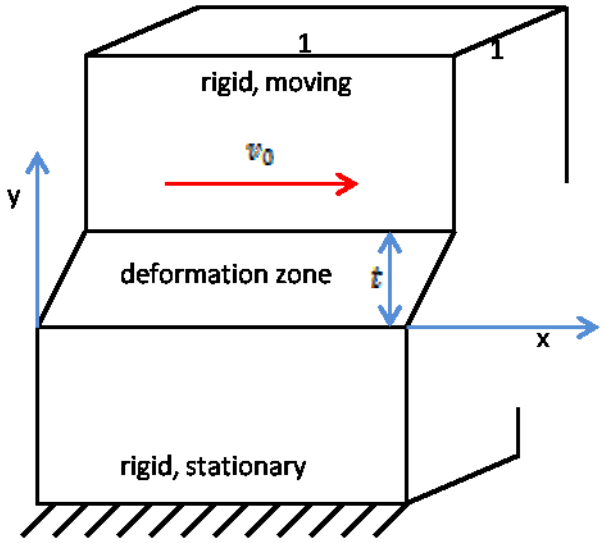

Figure 12. Idealized deformation in a slip surface (Murff, 2008)

The velocity components of the deformation zone in each direction due to the relative velocity are (Murff, 2008):

$$v_x = \frac{v_0}{t} y \qquad \text{Equation (18)}$$

$$v_y = v_z = 0 \qquad \text{Equation (19)}$$

Thus, the only non-zero strain rate terms are $\dot{\gamma_{xy}}$ and $\dot{\gamma_{yx}}$ (Murff, 2008):

$$\dot{\gamma_{xy}} = \dot{\gamma_{yx}} = \frac{1}{2}\left(\frac{\partial v_x}{\partial y} + \frac{\partial v_y}{\partial x}\right) = \frac{1}{2}\frac{v_0}{t} \qquad \text{Equation (20)}$$

The dissipation rate per unit volume can be written in terms of Tresca yield criterion as (Murff, 2008):

$$\dot{D} = s_u\left(2\dot{\gamma}_{xy}{}^2 + 2\dot{\gamma}_{yx}{}^2\right)^{1/2} = 2s_u\dot{\gamma}_{xy} = s_u\frac{v_0}{t} \qquad \text{Equation (21)}$$

Integrating over the entire volume gives the total dissipation (Murff, 2008):

$$\dot{D} = \int_{x=0}^{1}\int_{y=0}^{t} s_u\frac{v_0}{t}\,dy\,dx = s_u\frac{v_0}{t}\cdot t = s_u v_0 \qquad \text{Equation (22)}$$

Therefore the total dissipation along a slip surface only depends on s_u and v_0 and not on the thickness of the deformation zone (Murff, 2008).

Generalized Stresses and Strains

Upper bound analysis of shallow foundations in this thesis is performed using generalized stresses and strains, as described by Prager (1959). This generalization considers the following for characterizing the yield of a rigid, perfectly plastic soil model (Han, 2002):

- Forces and moments are treated as generalized stresses
- Interactions between forces and moments are treated as generalized yield surfaces
- Displacements and rotations are treated as generalized strains
- The generalized strains are the work conjugates of the generalized stresses (Prager, 1959)

As previously discussed, stresses and strains in plastic limit analysis can be related through the associated flow rule. This also holds true for generalized stresses and strains. This allows the calculation of dissipation rates, which can be shown to be a

function of the soil resistances (generalized stresses) and kinematically admissible velocity fields (generalized strains) (Han, 2002). This is further discussed in the Proposed Analysis chapter of this thesis.

Application of Upper Bound Method to Geotechnical Design

The upper bound method of plasticity has been applied to offshore geotechnical engineering designs in undrained soil, including:

- Retaining walls (Heyman, 1973)
- Bearing capacity of shallow foundations (Davis and Booker, 1973, and others)
- Shallow foundations subjected to torsional loads (Murff and Aubeny, 2011)
- Slope stability (Drucker and Prager, 1953 and Gibson and Morgenstern, 1962)
- Laterally loaded piles (Aubeny and Murff, 2001, Randolph and Houlsby, 1984, and Murff and Hamilton, 1993)
- Pipeline penetration (Murff, Wagner, and Randolph, 1989)

Use of the upper bound method of plasticity as an analysis tool for complex bearing capacity problems has been validated through checks with empirical solutions and few known exact solutions available, as well as providing insight into the failure mechanism (Murff and Miller, 1977-1).

The method by Davis and Booker (1973), which was previously discussed in this thesis, uses the upper bound method of plasticity to compute the bearing and overturning capacity of shallow foundations installed in clay soil with a linearly increasing undrained shear strength profile.

Others have applied the upper bound method to compute the bearing capacity of shallow foundations including:

- Determining the bearing capacity in nonhomogeneous soils (Murff and Miller, 1977-1, Murff and Miller, 1977-2, and Gourvenec and Randolph, 2003)
- Analyzing the effect of the embedment on bearing capacity and the failure envelope (Gourvenec, 2008, Yun and Bransby, 2007-1, and Yun and Bransby, 2007-2)
- Determining the shape of the failure envelopes based on footing geometry (Gourvenec, 2007-1 and Gourvenec, 2007-2)

The works referenced here apply the upper bound method to embedded shallow foundations of simple geometries (strip, circular, square, and rectangular footings). Bearing and overturning behaviors predicted by the upper bound method have been shown to compare favorably to those computed by FEM when investigating the effects of embedment of shallow foundations (Yun and Bransby, 2007-2).

Upper Bound Approach to Bearing and Overturning Capacity

If we consider a shallow foundation with some external vertical load applied, we can assume a failure mechanism through the soil and a virtual velocity in the direction of failure. In a 2-D analysis, the length of the failure mechanism will be a function of the location of an assumed axis of rotation, about which the foundation rotates due to the external load.

The internal dissipation rate of this system will be the product of the strength integrated over the failure surface, the length of the failure surface, and the virtual velocity. The work rate from the applied loads is the product of the applied stresses, the areas to which the stresses are applied, and the virtual velocity.

Let us consider a rectangular mudmat foundation with a vertical load, F_v, applied at an eccentricity, x_e (Figure 13 and Figure 14).

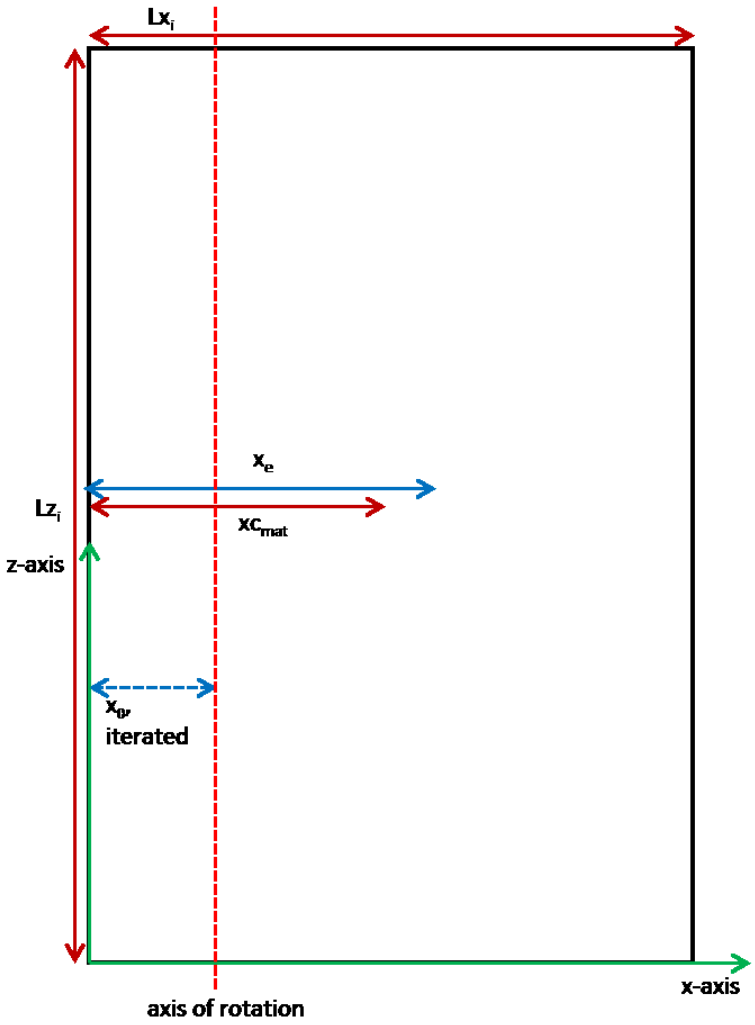

Figure 13. Plan view schematic of mudmat for upper bound method analysis

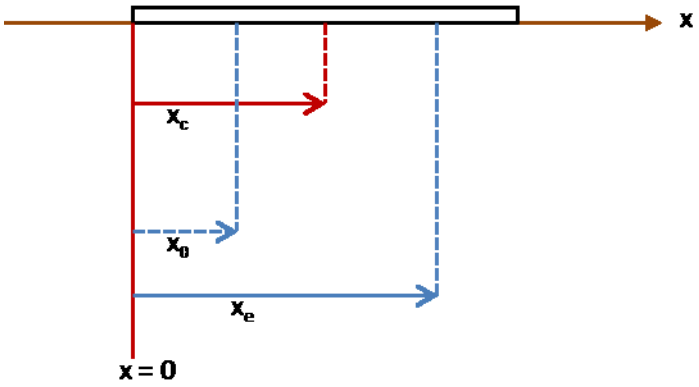

Figure 14. Side view of schematic of mudmat for upper bound approach analysis

The ultimate bearing capacity for the foundation can be calculated through an appropriate method (such as the previously discussed methods from API) based on the soil conditions. When we introduce an eccentric load, we can use the upper bound approach to compute the reduced bearing capacity and corresponding overturning capacity

The external work rate due to the eccentric load can be expressed as:

$$\dot{E} = F_v(x_e - x_0)\dot{\beta} \qquad \text{Equation (23)}$$

A proposed equation for the interaction surface is as follows (Murff, 2008):

$$f(Q, M) = Q^2 - Q_0 Q + 2Q_0\left(\frac{M}{B}\right) = 0 \qquad \text{Equation (24)}$$

The upper bound method of plasticity assumes a virtual rotation rate and displacement rate for each footing according to the applied load. The virtual rotation rate, $\dot{\beta}$, and virtual displacement rate, $\dot{\delta_v}$, are shown in Figure 15.

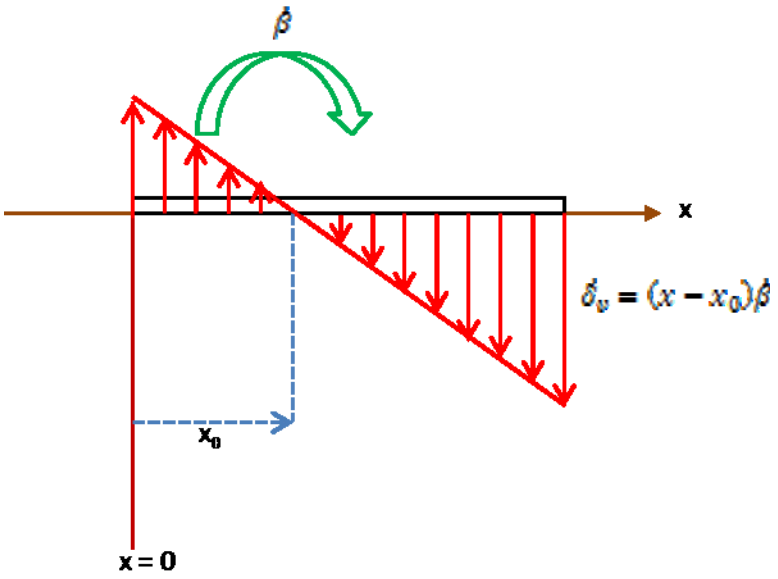

Figure 15. Virtual rotations and displacements for upper bound approach analysis

The virtual rotation rate at the axis of rotation can be related to the virtual displacement rates of each footing through the expressions:

$$\dot{\theta} = \frac{\partial f(Q,M)}{\partial M} = \frac{2Q_0}{B} = \dot{\beta} \qquad \text{Equation (25)}$$

$$\dot{\delta_v} = \frac{\partial f(Q,M)}{\partial Q} = 2Q - Q_0 = (x_i - x_0)\dot{\beta} \qquad \text{Equation (26)}$$

Using Equation (25) and (26) above, we can use the ratio of the virtual displacement rate to the virtual rotation rate to solve for the bearing capacity of the footing due to an eccentric load:

$$Q_i = Q_{0i} \cdot \left(\frac{1}{2} + \frac{x_c - x_0}{L_{xi}}\right) \cdot \sqrt{1 - \frac{N_s}{N_{smax}}} \qquad \text{Equation (27)}$$

Equation (27) reduces the ultimate bearing capacity of the footing by the shear demand to resist lateral loads and the location of the axis of rotation. As seen in Figure 15, the part of the footing that is on the "left" side of the axis of rotation (opposite the applied eccentric load) does not contribute to the calculated bearing capacity, although it will contribute to the corresponding overturning capacity.

We limit the bearing capacity of the footing to the ultimate bearing capacity, Q_{0i}, for no applied eccentric load. Therefore, Equation (27) is subject to the following constraints:

- $Q_i = 0$ if $Q_i < 0$ (does not contribute to bearing capacity)
- $Q_i = Q_i$ if $0 < Q_i < Q_{0i}$
- $Q_i = Q_{0i}$ if $Q_i > Q_{0i}$

We can now substitute Q_i into Equation (24) and solve for the moment capacity of the footing, M_i:

$$M_i = L_{xi}\left[\frac{Q_i}{2} - \frac{Q_i^2}{2Q_{0i}}\right] \qquad \text{Equation (28)}$$

The total internal energy dissipation rate for the footing can be expressed as:

$$\dot{D} = [Q_i(x_i - x_0) + M_i] \cdot \dot{\beta} \qquad \text{Equation (29)}$$

Finally, we can equate the internal energy dissipation rate to the external work rate by the applied eccentric load in Equation (23). By canceling the virtual rotations, $\dot{\beta}$, we solve for the vertical load at a specified eccentricity for the mudmat foundation:

$$F_v = \frac{Q_i(x_i - x_0) + M_i}{x_e - x_0} \qquad \text{Equation (30)}$$

When Equation (30) is minimized with respect to the location of the axis of rotation, x_0, the resultant force is the bearing capacity of the mudmat foundation for a given eccentricity.

The corresponding overturning capacity can be calculated as:

$$M = F_v(x_e - x_c) + \frac{x_0^2}{4} \cdot \alpha \cdot s_u \cdot L_z \qquad \text{Equation (31)}$$

Equation (31) is the sum of two components:

- Bearing capacity of the foundation multiplied by the assumed eccentricity
- Adhesion of the soil to the foundation base during uplift, assuming a semicircular slip surface (after Equation (4))

The value of the adhesion factor should vary from 0 to 1. A value of $\alpha = 0$ should be used for conservative estimates of bearing and overturning capacity when little

to no tension between the mat and soil surface is expected. Higher values of adhesion ($0 < \alpha < 1$) should be used when rapid loading or pull-out is expected.

Like Equation (27), which is limited to the ultimate bearing capacity of the footing, Equation (31) is limited to the maximum overturning capacity of the footing, which is calculated previously in Equation (4).

The free body diagram with the soil reactions can be seen in Figure 16. This figure shows the location of the axis of rotation, along with the bearing and uplift portions of the footing about this axis. The bearing pressure beneath the mat is constant, and the adhesion on the uplift portion of the mat applies a resisting moment to the eccentric load, F_v, applied at point x_c.

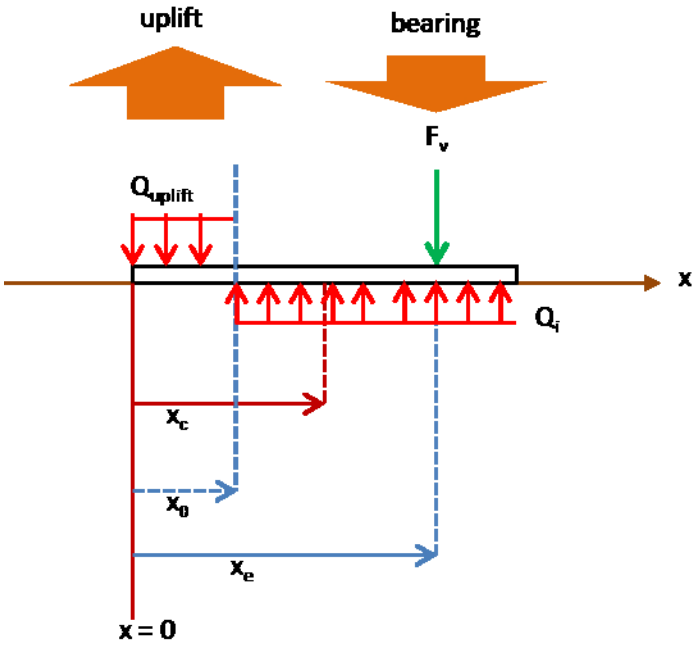

Figure 16. Free body diagram of mudmat for upper bound approach analysis

We can plot a complete interaction diagram by moving the location of the eccentric load from the centroid of the mudmat to the edge of the mudmat (i.e., $x_e = \frac{B}{2}$ to B). When the vertical resultant load is applied at the centroid of the footing, there is no eccentricity and the foundation is in pure bearing. When the resultant load is applied at the edge of the footing, the load is purely eccentric and there is zero bearing capacity of the foundation.

Comparison to Existing Methods

When we analyze a simple rectangular footing using the upper bound approach and assuming no adhesion during uplift, we will calculate the exact bearing and

overturning interaction as we would using existing methods. This is because the optimized location of the axis of rotation in the upper bound approach is equal to $2e$, from the effective area method (Equation (6) and Equation (7)). Thus, the effective bearing areas of the foundation calculated by both methods are the same.

Figure 17 shows a comparison of a 15 ft by 30 ft rectangular footing assuming a constant undrained shear strength profile (100 psf) calculated after:

- API RP 2A (2010)
- The upper bound approach (no adhesion or shear demand)
- The upper bound approach (full adhesion, no shear demand)

As seen in Figure 17, the overturning capacity of the mudmat foundation increases when adhesion is assumed between the footing base and the soil. This "tension" between the soil and footing applies a resisting overturning moment which allows the foundation to reach its maximum overturning capacity.

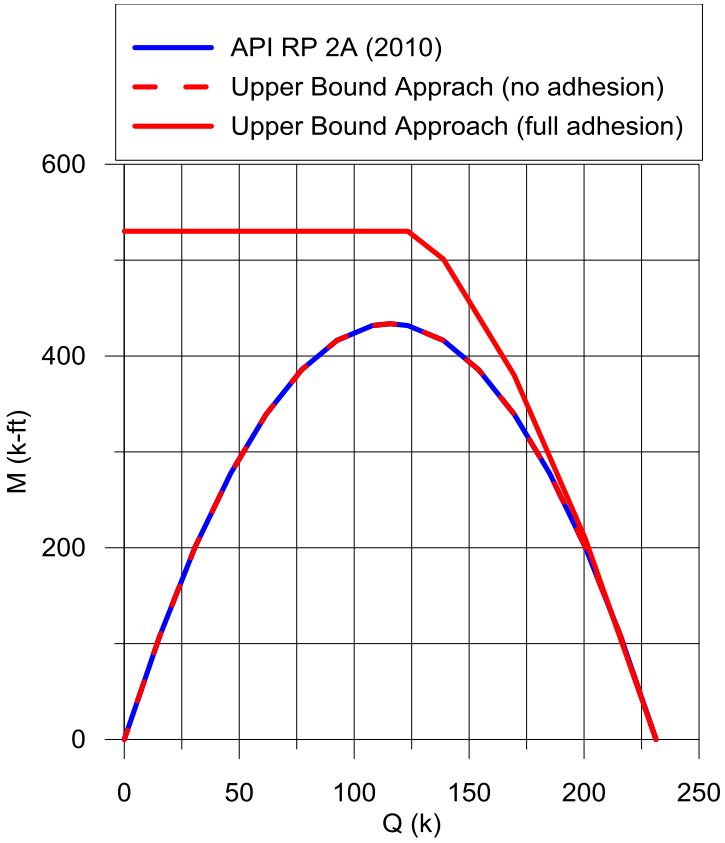

Figure 17. Example interaction diagrams (assume no shear demand)

PROPOSED ANALYSIS

The upper bound approach can be applied to shallow foundations with complex shapes that make bearing and overturning computations difficult with existing methods without the use of FEM.

METHOD OF ANALYSIS USING UPPER BOUND APPROACH

This approach employs the following steps, which are further explained in the following sections:

1. Divide the foundation into a series of n rectangular areas with appropriate dimensions based on the geometry of the mudmat (L_{xi}, L_{zi}, x_i) as shown for the "sled" foundation in Figure 18.

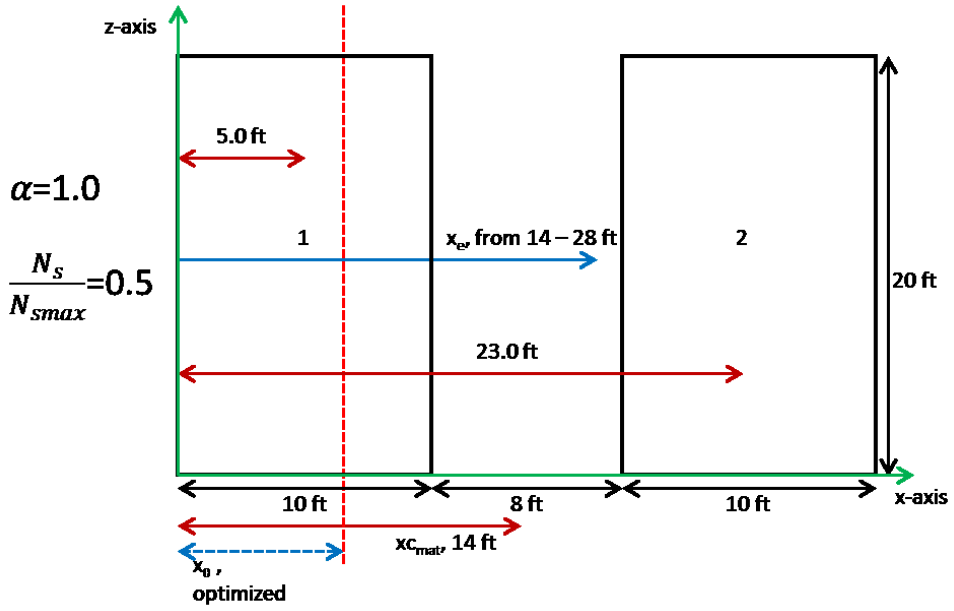

Figure 18. Discretization of a complex sled-shaped foundation

2. Assume a location of the applied eccentric load (x_e), a location for the virtual axis of rotation (x_0), an adhesion factor for mudmat uplift (α), and the shear demand due to sliding ($\frac{N_s}{N_{smax}}$)
3. Calculate an operative bearing pressure under the foundation based on the undrained shear strength profile. ($\frac{Q_{0i}}{A'}$). Equations (1) or (2) may be used for this purpose, with adjustments to the bearing factor based on the shear demand due to sliding and the eccentric load. They are reasonable estimates in the sense that they will provide exact values of bearing pressure for the case of pure vertical loading of a strip footing. While there is no guarantee that they are appropriate for arbitrary mudmat shapes, subsequent comparisons to finite element

calculations show that the operative bearing pressure estimated in this manner is not unreasonable.

4. Calculate the equivalent bearing capacity of each rectangular footing with respect to the virtual axis of rotation (Q_i, using Equation (27)), subject to the constraints that the equivalent bearing capacity cannot be greater than the bearing capacity in Step 3 and any capacity computed to be less than 0 does not contribute to bearing capacity. For footings that are discontinuous across the foundation width (footings 1 and 2 in Figure 18), the bearing capacities calculated by Equation (27) should be further adjusted for their manner of displacement (i.e. pure displacement to pure rotation). This should be a function of the distance of the centroid of these elements to the virtual axis of rotation (from Figure 18). The equation for this reduction is shown below, where Q_i is the capacity calculated from Equation (27).

$$Q_{ei} = Q_i \cdot \frac{N_{pi}}{2 + \pi} \qquad \text{Equation (32)}$$

The resulting free body diagram for the example sled foundation is shown in Figure 19. As shown, the bearing capacity of the footing closest to the axis of rotation (Footing 1) is lower than Footing 2, since the bearing factor is for pure rotation is lower than that for translation. The resistance to uplift due to the adhesion of the soil to the foundation base creates a moment that resists overturning due to the applied eccentric load.

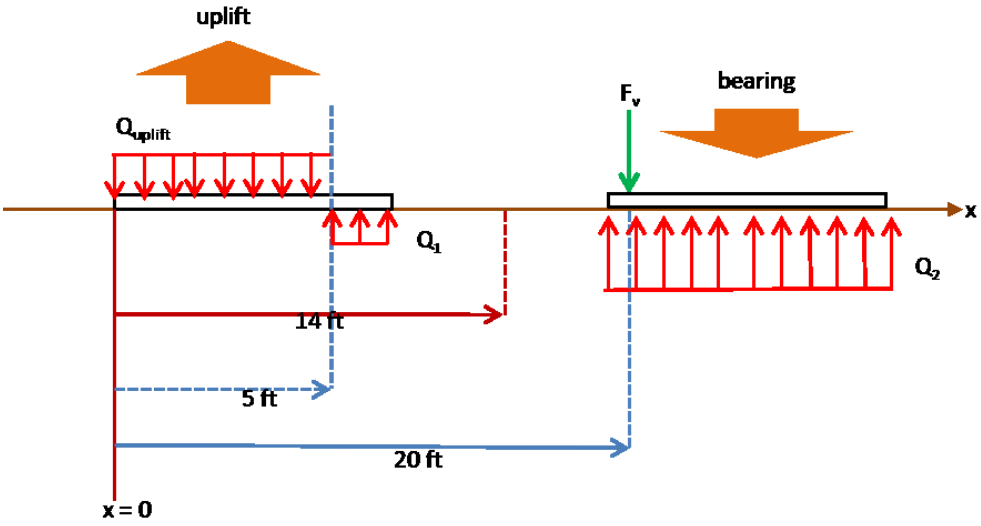

Figure 19. Free body diagram of eccentrically loaded sled foundation

5. Calculate the internal moment for each footing with respect to virtual axis of rotation (M_i, using Equation (28))
6. Sum the total internal energy dissipation rates for all n footings ($\dot{D}$, using Equation (29))
7. Divide the total internal energy dissipation rate by the distance of the location of the eccentric load to the virtual center of rotation and minimize with respect to x_0 to get the bearing capacity of the mudmat (F_v, using Equation (30))
8. Calculate the corresponding moment capacity (M, using Equation (31))
9. Select a new location of x_e and repeat Step 2 through Step 9 until a full interaction diagram can be plotted

The following sections give a detailed explanation of each step, show supporting plots, and work through a sample calculation for the sled foundation installed in soil with a constant undrained shear strength profile (100 psf).

INPUT OF GEOMETRY AND LOADING CONDITIONS

For Step 1 of this analysis, we discretize the sled-shaped mudmat foundation of into a series of n rectangular footings of width L_{xi}, length L_{zi}, and a centroid in the X-direction of x_i, shown in Figure 20.

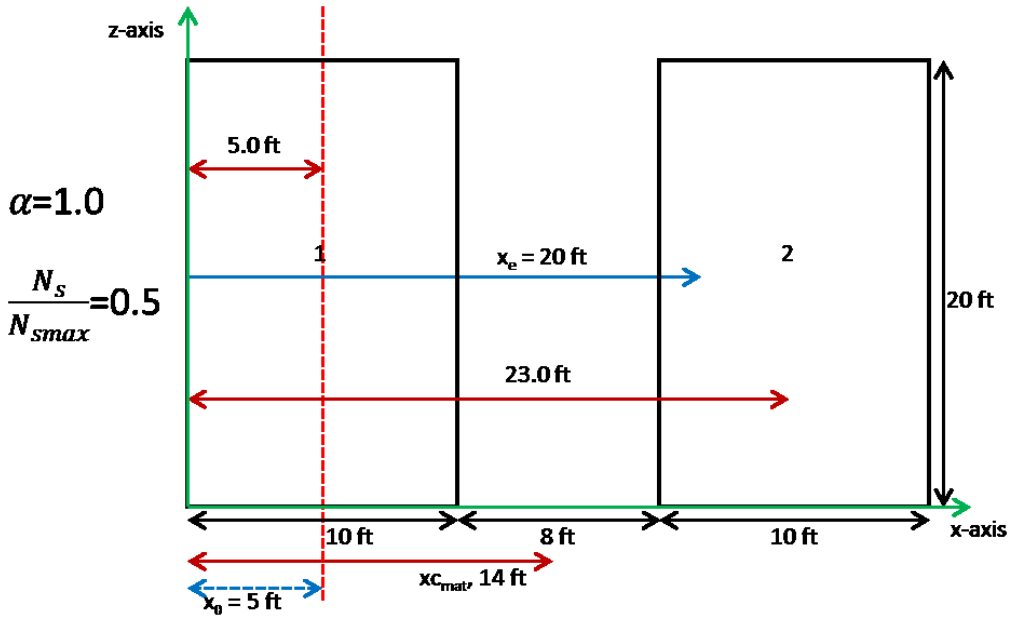

Figure 20. Discretized sled-shaped foundation with eccentric load and axis of rotation

For Step 2 of this analysis, we will assume an eccentric load applied at $x_e = 20\,ft$ from the edge of the mat. As shown in Figure 20, we will assume full adhesion of the soil to the base of the footing and a shear demand of $\frac{N_s}{N_{smax}} = 0.5$ due to resist lateral loads.

We will also assume some location of the axis of rotation for this foundation, $x_0 = 5\,ft$. The velocity field about this axis is shown in Figure 21.

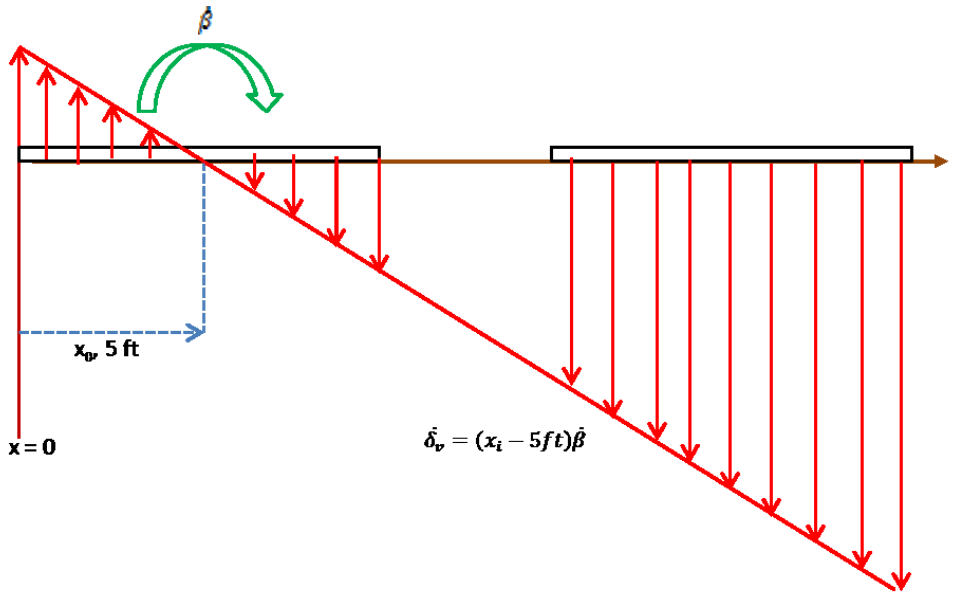

Figure 21. Virtual velocity field for example sled foundation

CALCULATION OF SOIL REACTIONS FOR DISCRETIZED FOOTINGS

Per Step 3 of this analysis, we can calculate the ultimate bearing capacity of each rectangular footing with no eccentric load, Q_{0i}, through one of the previously described methods from API, depending on the undrained shear strength profile. As previously noted, the operative bearing pressure beneath the mat due to the eccentric load is uniform.

Since both footings are of the same dimensions, the ultimate bearing capacities will be equivalent. Using Equation (1) for a constant undrained shear strength profile, we calculate the bearing capacity of each footing to be:

$$Q_0 = [(100psf\ )(5.14)(1)](10\ ft)(20\ ft) = 102.8\ k$$

For Step 4 of this analysis, we will calculate the effective bearing capacity of each footing, including applying a reduction based on the location of each footing from the axis of rotation since the bearing surface is not continuous.

From Equation (27), we calculate the effective bearing capacity of each footing to be:

$$Q_1 = (102.8\ k) \cdot \left(\frac{1}{2} + \frac{5\ ft - 5\ ft}{10\ ft}\right) \cdot \sqrt{1 - 0.5^2} = 44.5\ k$$

$$Q_2 = (102.8\ k) \cdot \left(\frac{1}{2} + \frac{23\ ft - 5\ ft}{10\ ft}\right) \cdot \sqrt{1 - 0.5^2} = 204.8\ k \rightarrow 102.8\ k$$

The effective bearing capacity of Footing 2, Q_2, was calculated to be higher than the ultimate bearing capacity of the footing, therefore we took the value of Q_2 to be the minimum of these two values (according to the constraints in Equation (27)).

From Figure 7, we can find the value of N_{pi} for each footing based on its distance from the axis of rotation. These are listed in Table 1.

Table 1. Adjusted bearing factors based on distance from axis of rotation

Footing	$\boldsymbol{\frac{x_i - x_0}{L_{xi}}}$	$\boldsymbol{N_{pi}}$
1	0.0	π
2	1.8	$2 + \pi$

The further reduction of the effective bearing capacity of each footing based on the location of the axis of rotation is calculated according to Equation (32):

$$Q_{e1} = (44.5\ k) \cdot \frac{3.14}{5.14} = 27.2\ k$$

$$Q_{e2} = (102.8\ k) \cdot \frac{5.14}{5.14} = 102.8\ k$$

The adhesion of the soil only acts on the base of Footing 1, therefore the resisting force due to this adhesion is:

$$(5\ ft) \cdot (20\ ft) \cdot (1.0) \cdot (100\ psf) \cdot (\pi) = 31.4\ k$$

Figure 22 shows the resulting free body diagram due to the eccentric load and the soil reactions.

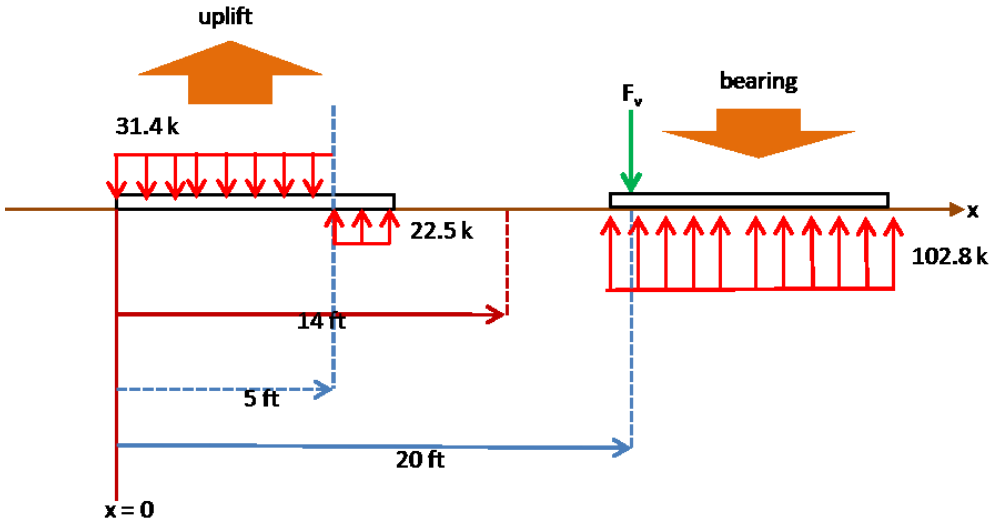

Figure 22. Soil reactions for example mudmat foundation

CALCULATION OF BEARING AND OVERTURNING CAPACITY FOR ENTIRE FOUNDATION

Following Step 7, we can calculate the energy dissipation rate of each footing and sum them for the total energy dissipation for the entire foundation using Equation (29). This dissipation is divided by distance from the location of the eccentric load to the virtual center of rotation (Step 8) and minimized with respect to x_0 to calculate the bearing capacity of the mudmat foundation through Equation (30). The corresponding overturning capacity is calculated in Step 9 by Equation (31).

For this example, the total dissipation rate of each footing and the total for the foundation are calculated assuming the location of the virtual axis of rotation is at

$x_0 = 5\ ft$ in Table 2. The total dissipation is minimized by x_0 and the optimized value of x_0 is given along with the corresponding bearing capacity and overturning capacity.

Table 2. Bearing and overturning capacity of example sled foundation

For $x_0 = 5\ ft$			
Element	$\boldsymbol{Q_i(x_i - x_0)}$ **(k-ft)**	$\boldsymbol{M_i}$ **(k-ft)**	$\boldsymbol{\dot{D}_i}$ **(k-ft· β̇)**
1	0	100	100
2	1850	0	1850
Total Dissipation, $\boldsymbol{\dot{D}}$ **(k-ft·** $\boldsymbol{\dot{\beta}}$**)**	1950		
Optimized $\boldsymbol{x_0}$ **(ft)**	6.69		
Bearing Capacity (k)	129.3		
Overturning Capacity (k-ft)	845.9		

INTERACTION DIAGRAM

Following Step 10, we can vary the location of the eccentric load from the centroid of the mudmat (pure bearing) to the trailing edge of the mudmat (pure overturning) and calculate the corresponding bearing and overturning capacities to form an interaction diagram.

The interaction diagram for the example sled is shown in Figure 23 and the points are listed in Table 3, along with the location of the eccentric load.Also plotted is the bearing and overturning interaction assuming no adhesion to the base of the footing for comparison.

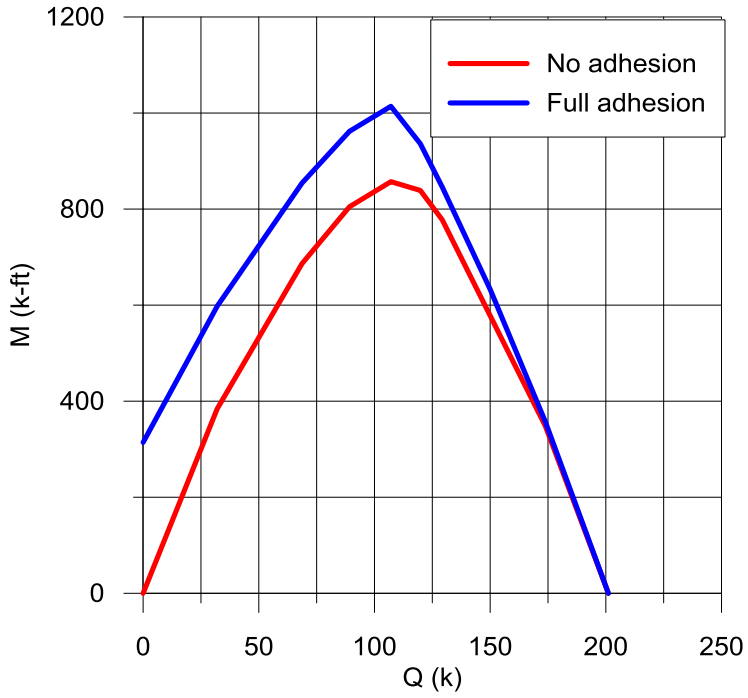

Figure 23. Interaction diagram for example sled foundation

Table 3. Points for the bearing-overturning interaction of the example sled foundation

Eccentric Load Location, x_e (ft)	Bearing Capacity, Q (k)	Overturning Capacity, M (k-ft)
14	201.1	0.0
16	173.9	356.7
18	150.0	632.9
20	129.3	845.9
21	119.8	936.2
22	107.1	1014.
23	89.2	961.4
24	68.7	854.3
26	32.0	597.7
28	0.0	314.2

FRAME EXAMPLE

We can analyze the bearing and overturning capacity of a frame-shaped mudmat (rectangular footing with a rectangular cut-out) by discretizing it into four rectangular footings as shown in Figure 25.

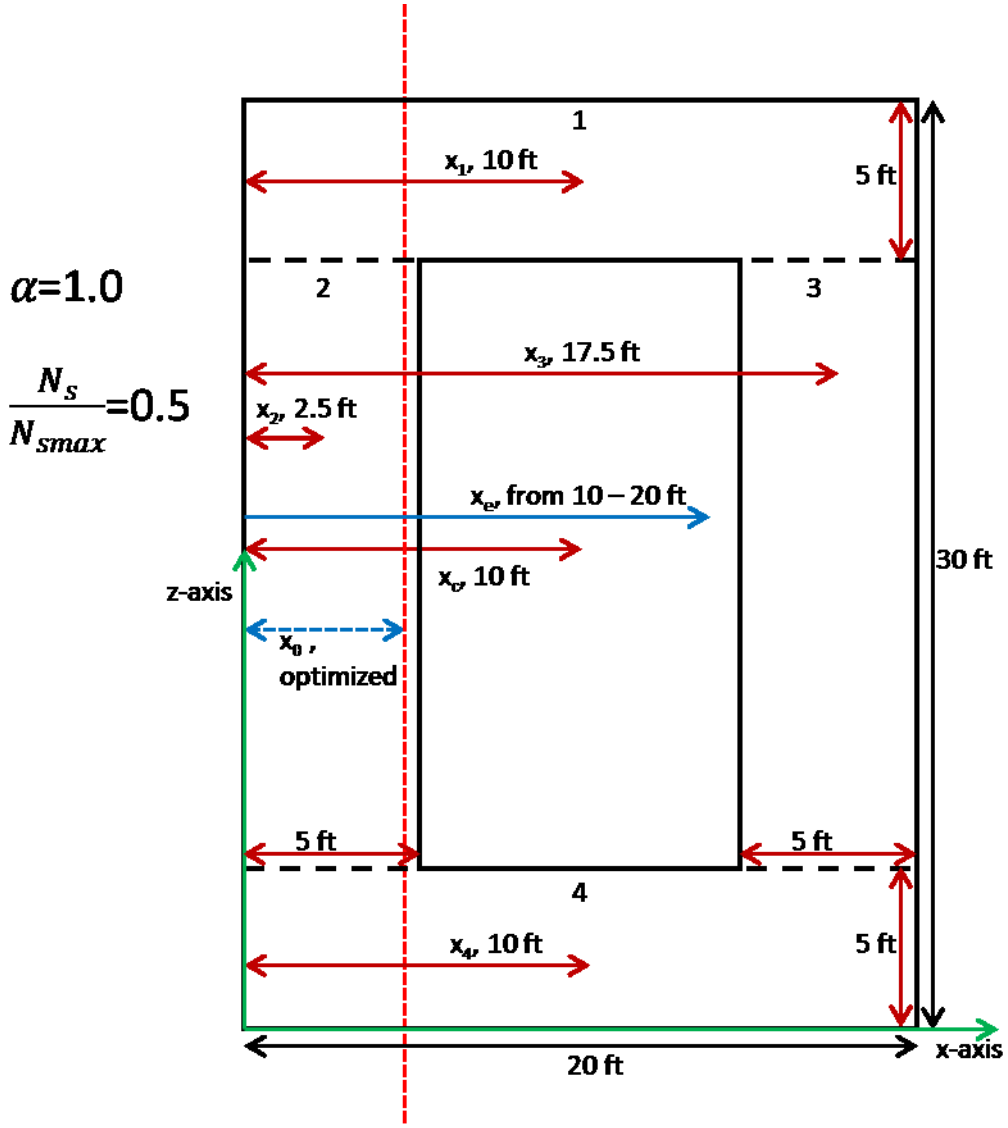

Figure 24. Discretized frame-shaped mudmat foundation with center cut-out

As shown in Figure 24, it is important to discretize a complex geometry in a way that keeps continuous, rectangular bearing areas across the foundation together (Footing 1 and Footing 4). This eliminates any potential interference of the bearing failure mechanisms that may otherwise be an artifact of the proposed analysis.

Assuming the foundation is installed in undrained soil with a constant undrained shear strength profile, $s_u = 100\,psf$, we can calculate the bearing and overturning interaction, as shown in Figure 25 (points shown in Table 4). Also plotted in this figure is the bearing and overturning interaction assuming no adhesion of the soil to the base of the footing.

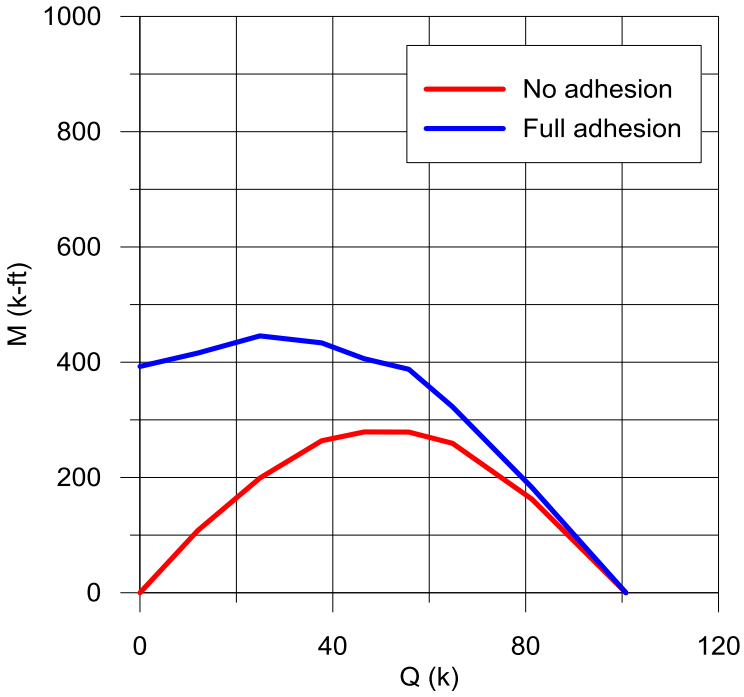

Figure 25. Interaction diagram for frame-shaped mudmat with center cut-out

Table 4. Points for the interaction for frame-shaped mudmat with center cut-out

Eccentric Load Location, x_e (ft)	Bearing Capacity, Q (k)	Overturning Capacity, M (k-ft)
10	100.8	0
12	81.27	182.9
14	64.83	322.7
15	55.76	387.8
16	46.51	406.1
17	37.67	433.6
18	24.88	445.7
19	12.00	415.9
20	0.0	392.7

VALIDATION THROUGH FEM

The force-moment interaction was calculated using the upper bound method of plasticity as previously described for a 10-ft-wide by 20-ft-long mudmat foundation on two undrained shear strength profiles:

- Constant undrained shear strength, $s_u = 100\ psf$
- Undrained shear strength of , $s_{u0} = 30\ psf$ at the seafloor, linearly increasing at a rate of $8\ psf/ft$.

The force-moment interaction of a mudmat foundation was analyzed on two undrained shear strength profiles using ABAQUS. This was done by evaluating the soil response to pure bearing displacement, pure overturning rotation, and a combination of displacements and rotations to generate an interaction diagram.

FINITE ELEMENT METHODS

The finite element method is a numerical way of solving for the stresses and deformations in a body by breaking that body into much smaller sub-regions (identified by nodes) that compose a mesh.

Finite element methods are used for analyzing complex geotechnical engineering problems. Several popular programs exist for finite element analysis of foundations, including ABAQUS and PLAXIS, among others. Finite element methods are described in the following sections, and ABAQUS is addressed specifically.

Background

Finite element methods have been used to analyze soil-structure interaction for many years. Many attribute the early development of FEM to the numerical analyses done by Courant and later by Argyris, Turner, Clough, and others (Gupta and Meek, 1996). Courant modeled St Venant's torsion of a square, hollow box using mesh subdivisions of up to nine triangular nodes (Courant, 1942).

As the computational power of computers improved, meshes were expanded to contain thousands of nodes. As the sub-regions in a mesh become smaller, the solutions given by FEM approaches should converge towards the analytical solution (Gupta and Meek, 1996).

FEM for structural analysis (in geotechnical engineering, the structure is the soil mass) generally involve the following steps (Sture, 2004):

- Establish stiffness relationships for the material (i.e. the elastic modulus and shear strength of the soil)
- Apply boundary conditions
- Divide the material into sub-regions represented by nodes, and enforce compatibility (all sub-regions are connected to form a continuous mesh)
- Enforce equilibrium conditions at each node
- Develop system of equations for all nodes in the mesh (called "assembling")
- Solve and system for all nodes

FEM has been used geotechnical engineering to predict the soil response during staged construction, excavations, and more. In shallow foundation analysis, FEM is used when the soil conditions and geometry becomes too complex to apply the simpler methods previously described.

FEM software for geotechnical analysis is used commercially, with the most popular programs being ABAQUS and PLAXIS in the offshore industry. Both of these programs allow for 2-D and 3-D analyses.

ABAQUS

ABAQUS was originally released in 1978 and is a popular FEM program for solving complex geotechnical engineering designs. In simple foundation design applications, ABAQUS allows users to define and assign properties to a soil mass and model the response to displacements and rotations.

DEFINING THE PROBLEM

ABAQUS allows the user to define the materials and boundary conditions for a FEM analysis. When analyzing a shallow foundation in 2-D, we need to define:

- The assembly of the soil mass (the location of the nodes in the mesh)
- The assembly of the foundation (the width location of the foundation on the soil mass)
- The sub-regions (elements) and the nodes that compose them
- The material properties for the soil (elastic modulus and plastic yield point)
- The material properties for the foundation (rigid, no deformation)

- The boundary conditions (the displacement and rotation of the foundation from its original location)

One can model a constant undrained shear strength profile by defining the soil mass to have the same material properties everywhere in the mesh. Alternatively, we can model a linearly increasing undrained shear strength profile by appropriately increasing the elastic modulus and plastic yield point with depth.

Since we are interested in the bearing and overturning capacity of a shallow foundation, we can model a range of eccentric loads by specifying rotations and displacements of the foundation. Ideally we want to view the interaction between an applied overturning moment and the bearing capacity of the foundation.

The user can model pure bearing by inputting a vertical displacement large enough to completely fail the soil and no rotation. Likewise, pure overturning is modeled by inputting a rotation large enough to completely fail the soil with zero average vertical displacement. These represent the maximum bearing and overturning capacities of the foundation. Finally, we can represent the interactions between vertical force and overturning moment by inputting combinations of vertical displacements and rotations.

The ABAQUS model used in this thesis included:

- The finite element mesh comprised 3,441 square elements with a total of 10,322 nodes (Figure 26).

- An elastic modulus, $E = 500s_u$, was used in the analyses. ABAQUS requires uniaxial compression strength to characterize yield. Uniaxial compression relates to undrained strength in simple shear according to the relationship $q_u = \sqrt{3}s_u$
- A Poisson's ratio of 0.35 was assigned to the soil to approximate undrained loading conditions.
- An elastic-perfectly plastic material with a von Mises yield criterion was assumed. Plastic deformations obey an associated flow law.
- Four-node linear interpolation elements were utilized with full integration.
- Loading was applied in a displacement control mode to a maximum vertical displacement of 1 ft for the case of pure translation and to a maximum rotation of 0.35 radians for the case of pure rotation.
- Imposed boundary constraints are shown in Figure 27.
- Collapse loads were taken as the magnitude of the ultimate reaction forces or moments associated with the imposed displacements.

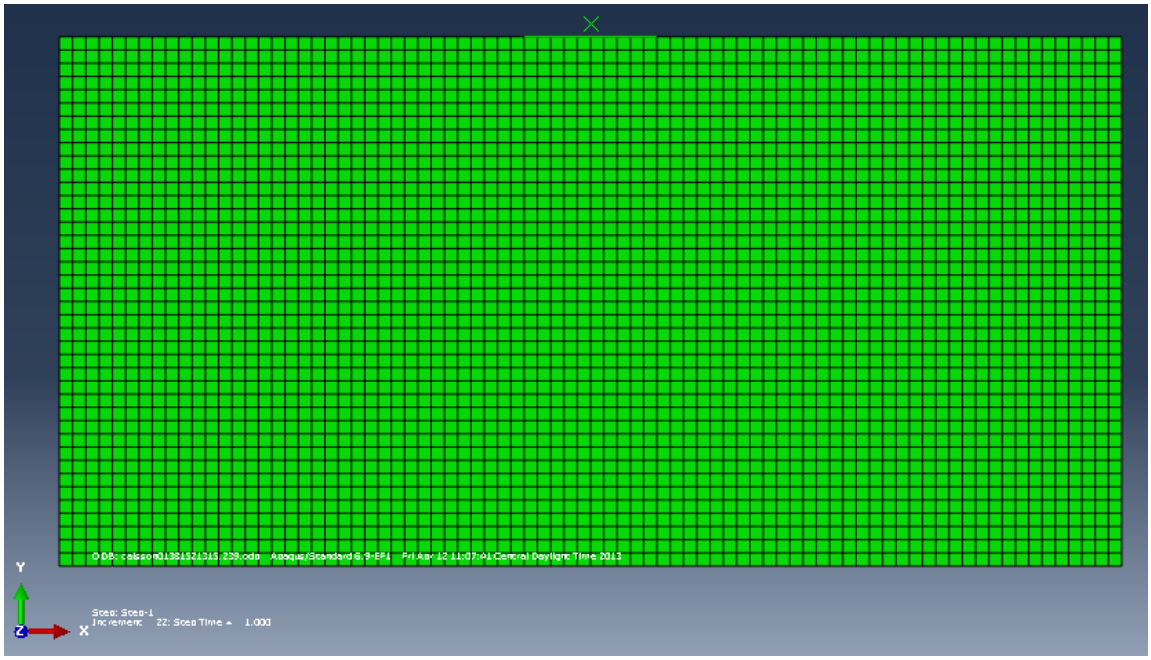

Figure 26. Original mesh, prior to displacements and rotations

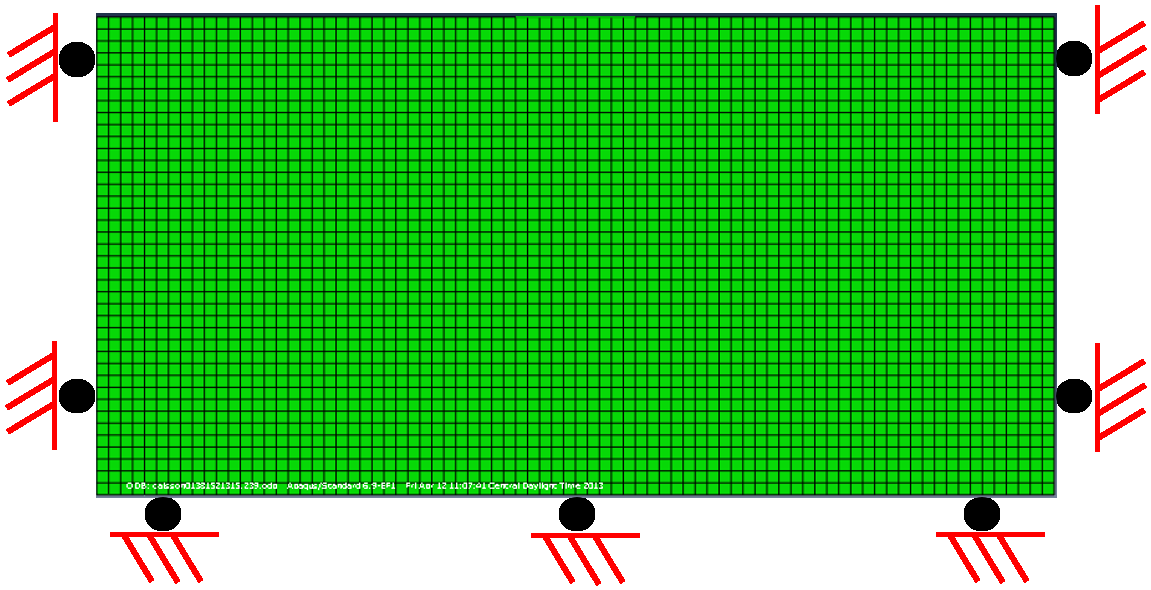

Figure 27. Original mesh, with applied boundary conditions

INTERPRETING THE RESULTS

An ABAQUS analysis produces several outputs, including a data file that can be read with a word processor and an output file that must be viewed in the ABAQUS CAE (Complete ABAQUS Environment).

The data file gives a detailed report of the analysis and reports requested information for user-specified nodes. When analyzing the force-moment interaction of a shallow foundation analysis, we view the vertical force and moment reaction applied to the foundation during the corresponding displacement and rotation. In a 2-D analysis this gives us the bearing capacity (in force per unit length) and corresponding overturning capacity (in force times length per unit length) for the specified displacement and rotation.

We can compute the total bearing capacity and overturning capacity by multiplying these values by the length of the foundation. An example of the force-moment interaction based on ABAQUS results is shown in Figure 28.

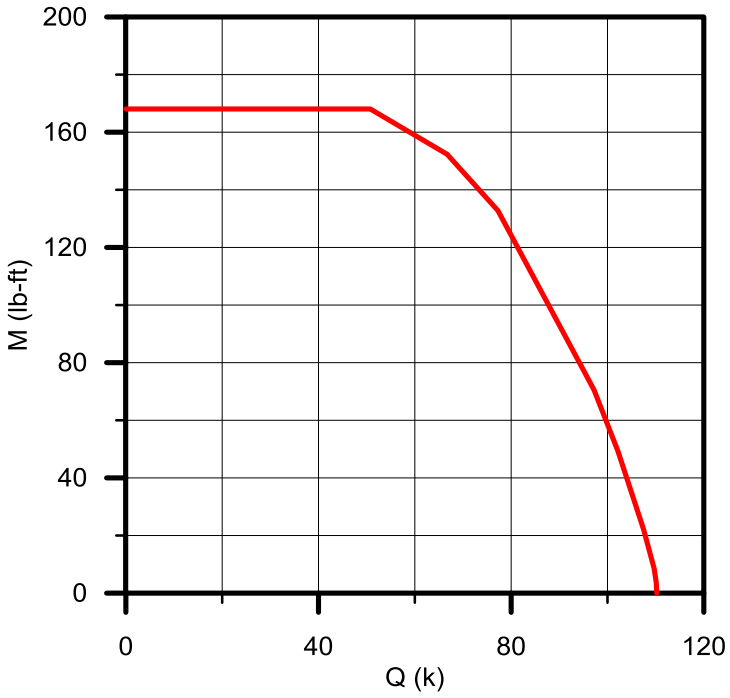

Figure 28. Interaction diagram for mudmat analyzed with ABAQUS

Note that the interaction diagram for the ABAQUS results does not decrease between zero overturning capacity and the maximum moment capacity, as seen in the interaction diagrams computed by the upper bound method. This is because ABAQUS calculates the soil reactions for given displacements and rotations, and was used to verify the maximum overturning and bearing capacities and their interaction from the maximum overturning to the maximum bearing capacity.

The output file viewed in CAE allows the user to view stress fields, strain, the final displaced mesh, and much more. Viewing these results allows us to see the failure

mechanism due to the applied displacements and rotations as well as the stress field imparted onto the soil mass. The deformed mesh is shown below in Figure 29.

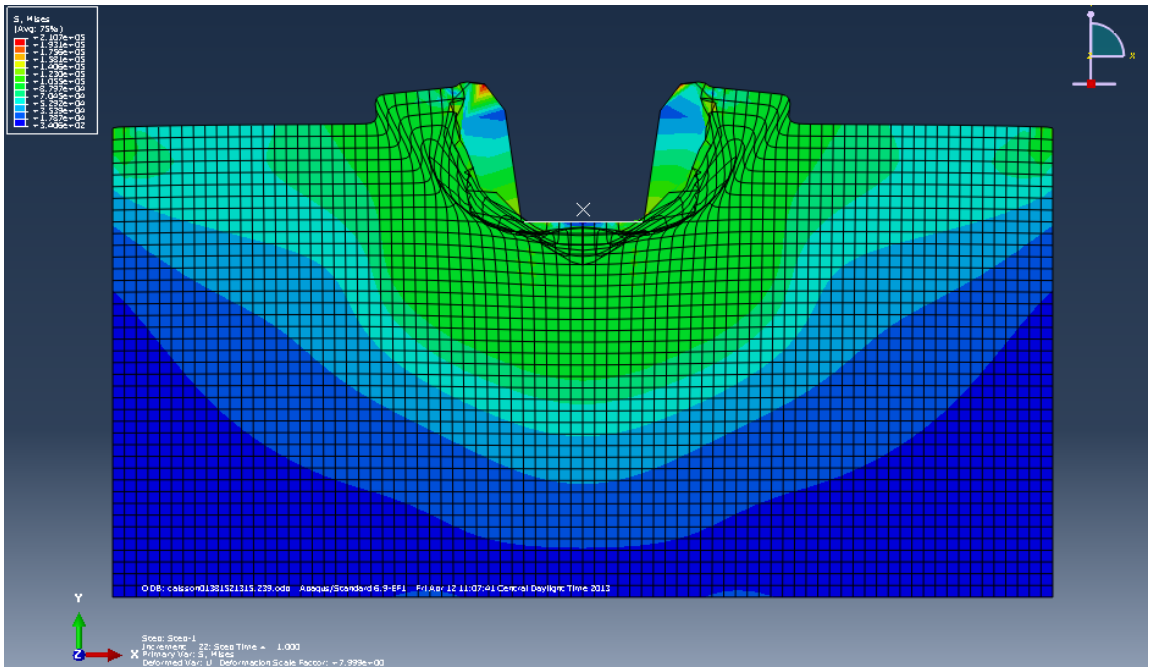

Figure 29. Deformed mesh for pure bearing with constant undrained strength

Figure 30 through Figure 35 show plots of the strain and Mises stress for pure bearing, a combination of bearing and overturning, and pure overturning for both soil profiles. From these plots, we can see the change in failure mechanism in the soil as a rotation is applied to the system, as would be the case with an overturning moment.

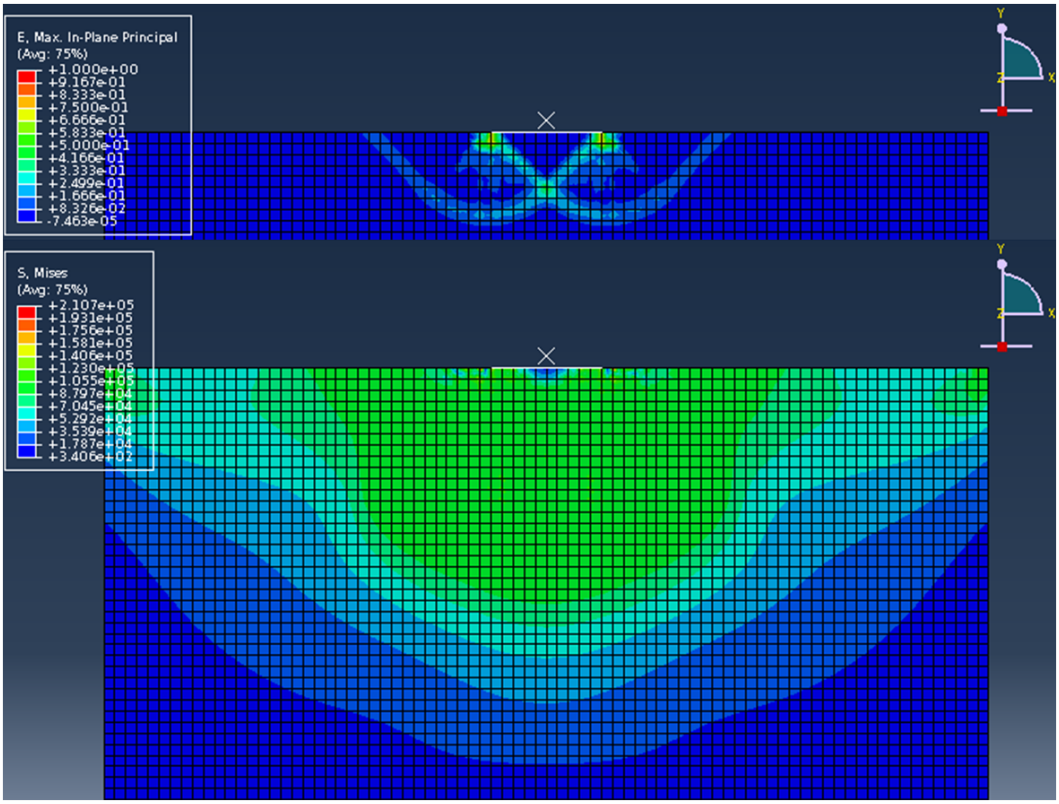

Figure 30. Strain and Mises stress for pure bearing (constant s_u)

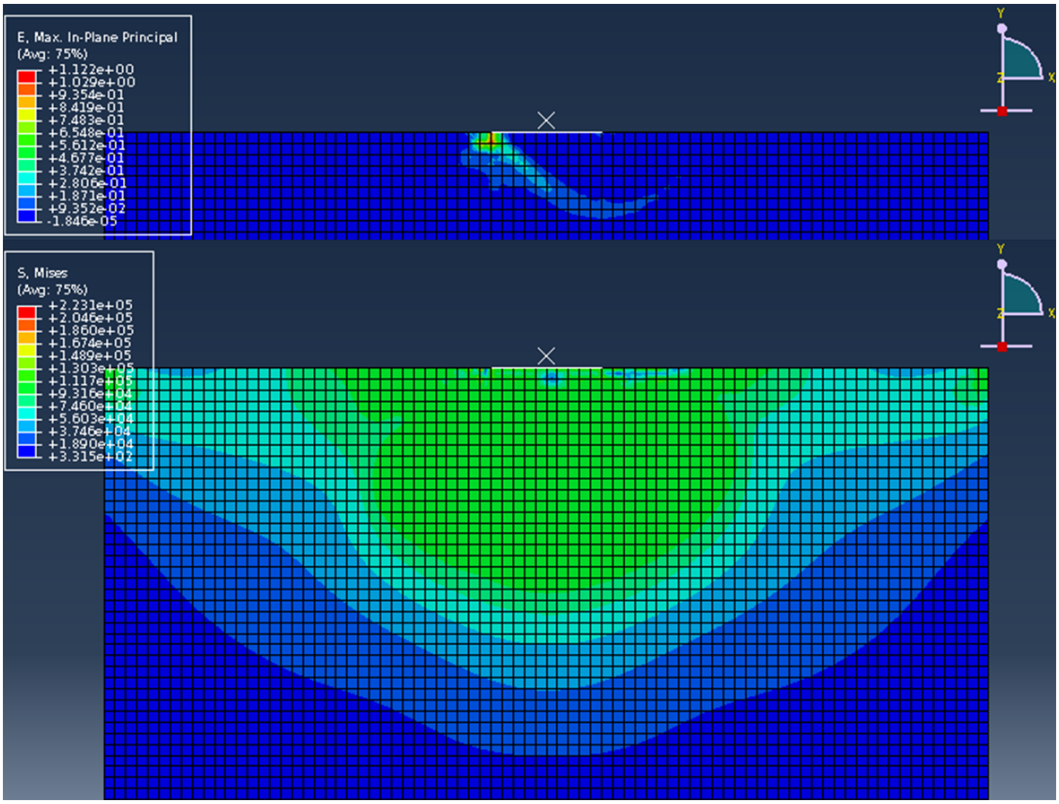

Figure 31. Strain and Mises stress for combined bearing/overturning (constant s_u)

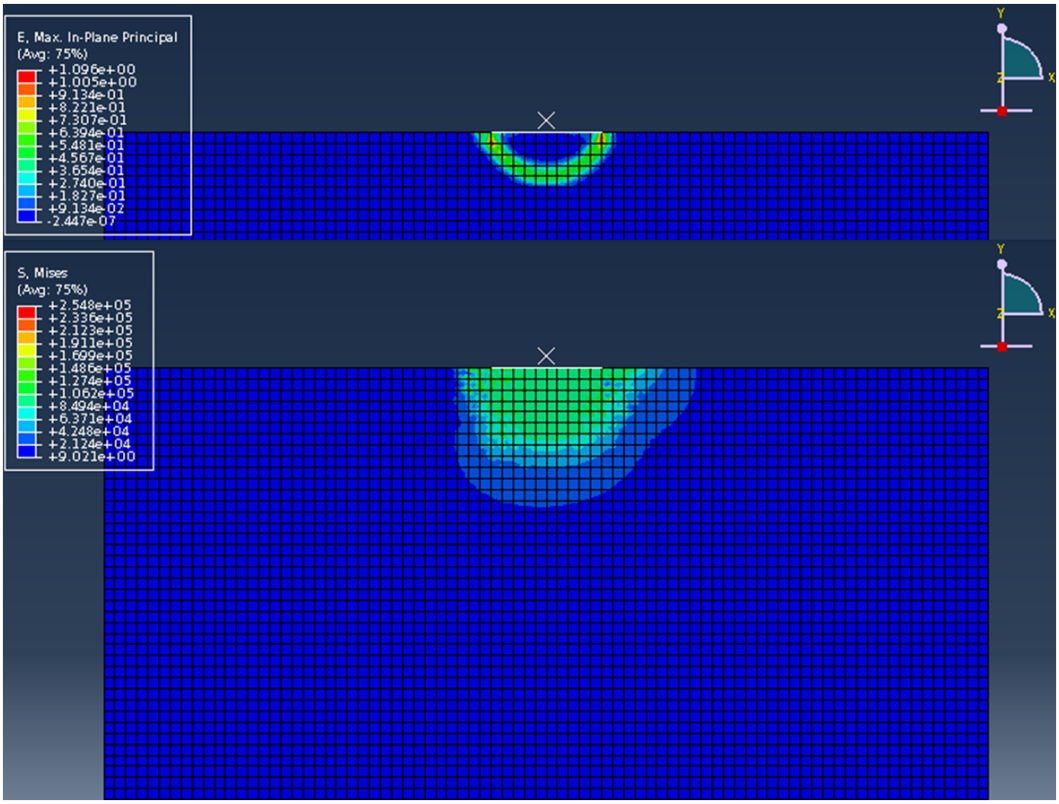

Figure 32. Strain and Mises stress for pure overturning (constant s_u)

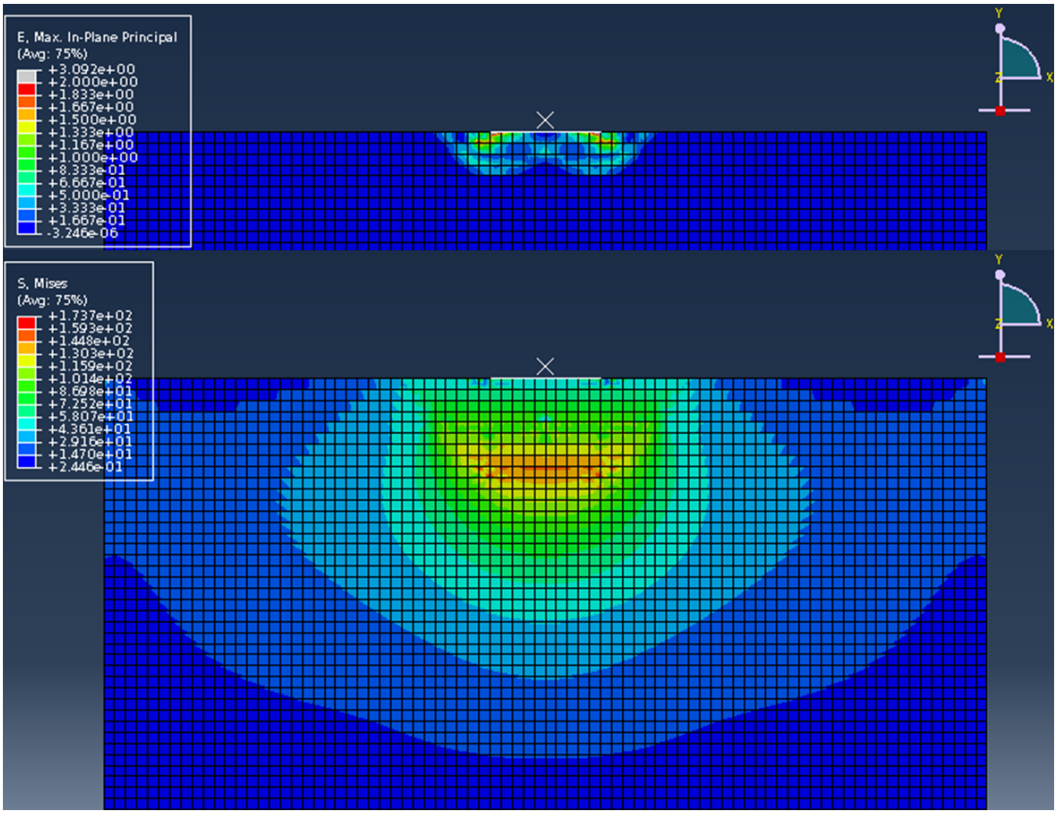

Figure 33. Strain and Mises stress for pure bearing (increasing s_u)

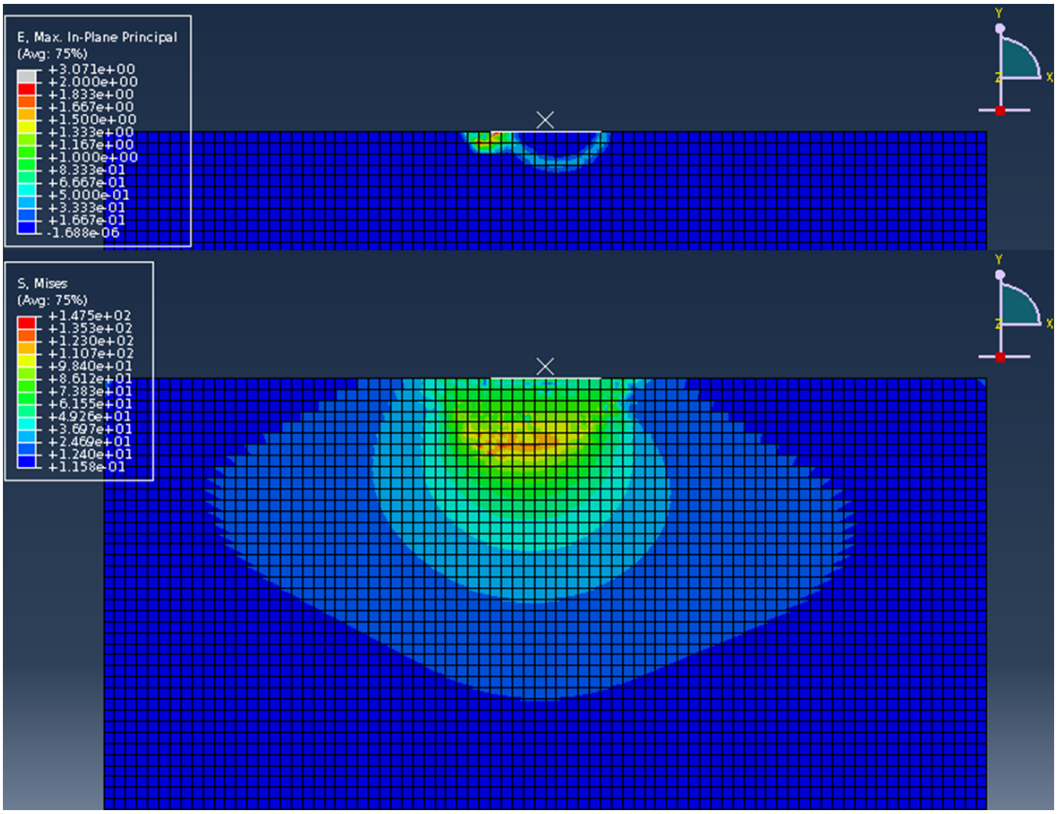

Figure 34. Strain and Mises stress for combined bearing/overturning (increasing s_u)

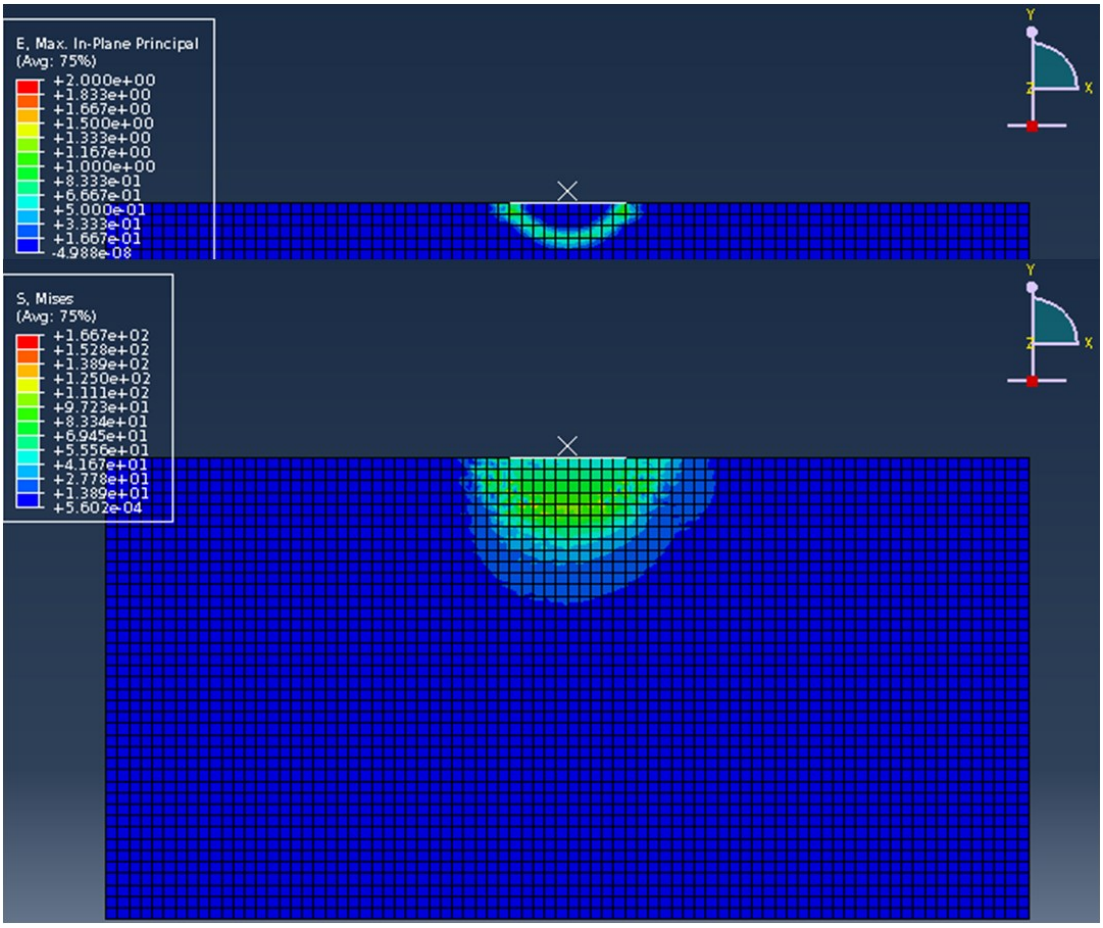

Figure 35. Strain and Mises stress for pure overturning (increasing s_u)

COMPARISON OF PROPOSED METHOD TO ABAQUS RESULTS

The results of the proposed analysis were compared to those of the ABAQUS analysis.

COMPARISON TO RAW ABAQUS RESULTS

The results of the analyses are plotted two ways:

- The magnitudes of the force-moment interaction
- The magnitudes of the force-moment interaction normalized by their corresponding maxima

Figure 36 and Figure 37 show force-moment interaction for both undrained shear strength profiles. As evident in the plots of the magnitudes, ABAQUS predicts higher bearing capacities and overturning capacities than the upper bound method of plasticity for both undrained shear strength profiles.

The normalized force-moment interaction plots show the ABAQUS and upper bound method results to closely match for the constant undrained shear strength profile. The normalized results for the linearly increasing undrained shear strength profile show greater normalized moment values to corresponding normalized force values.

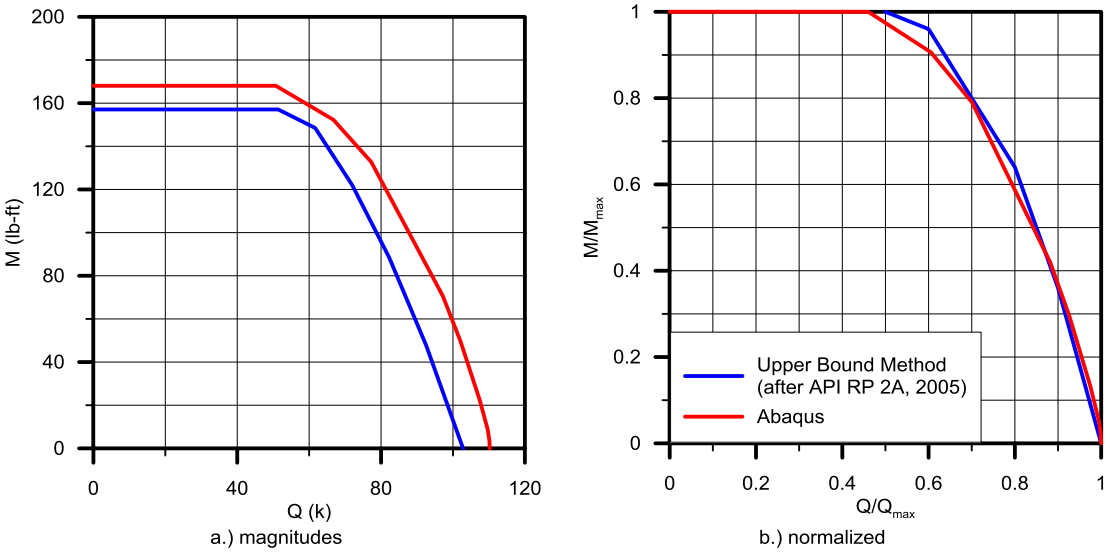

Figure 36. Comparison of results for constant s_u (raw ABAQUS results)

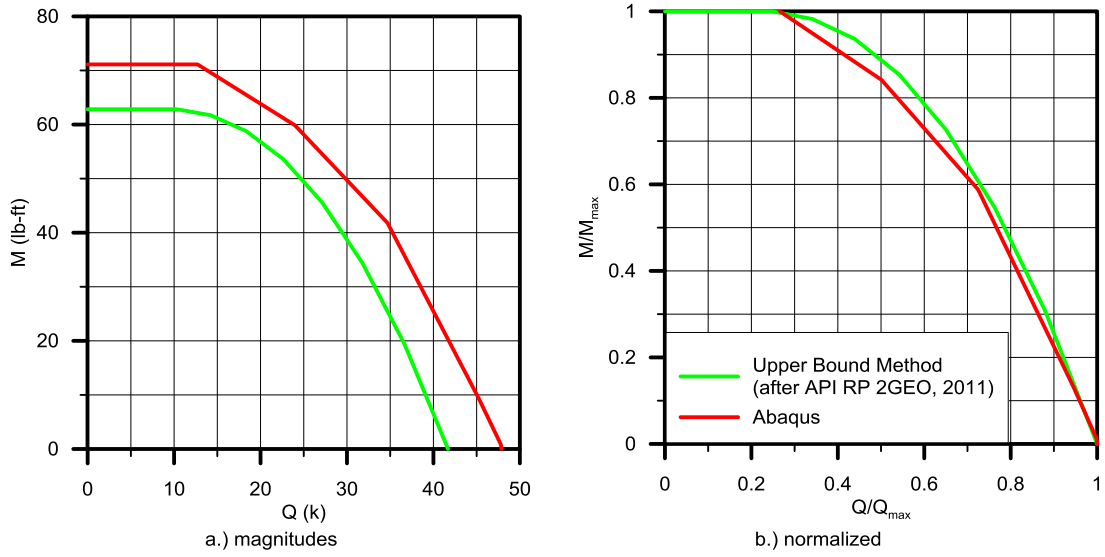

Figure 37. Comparison of results for linearly increasing s_u (raw ABAQUS results)

COMPARISON WITH CALIBRATED ABAQUS RESULTS

The ABAQUS results were adjusted based on known bearing and overturning capacity factors that would be expected for this type of analysis.

The bearing capacity factors were calculated from the pure bearing capacities predicted by ABAQUS for both undrained shear strength profiles. For both profiles, the bearing capacity factors derived from the ABAQUS results are higher than $2 + \pi$. Table 5 presents the results of this check.

The overturning capacity factors were calculated from the pure overturning capacities predicted by ABAQUS for both undrained shear strength profiles. For both profiles, the overturning capacity factors derived from the ABAQUS results are higher than $\frac{\pi}{4}$. Table 5 presents the results of this check.

This check was used to calibrate the ABAQUS results by reducing the force and moment values by the percentage indicated by the calculated factors. This reduction is shown in Table 5 for both undrained shear strength profiles.

Table 5. Calibration reductions for ABAQUS results

Strength Profile	N_c	N_c, **ABAQUS**	**Percent Reduction**	N_m	N_m, **ABAQUS**	**Percent Reduction**
$100 \cdot psf$	5.14	5.512	6.75 %	$\frac{\pi}{4}$	0.840	6.53 %
$30 \cdot psf + 7 \cdot \frac{psf}{ft}$	5.14	5.983	14.08 %	$\frac{\pi}{4}$	0.889	11.65 %

Figure 38 plots the magnitudes of the calibrated ABAQUS predictions with those of the upper bound approach. The plots show close agreement between the upper bound approach and the ABAQUS results for both profiles.

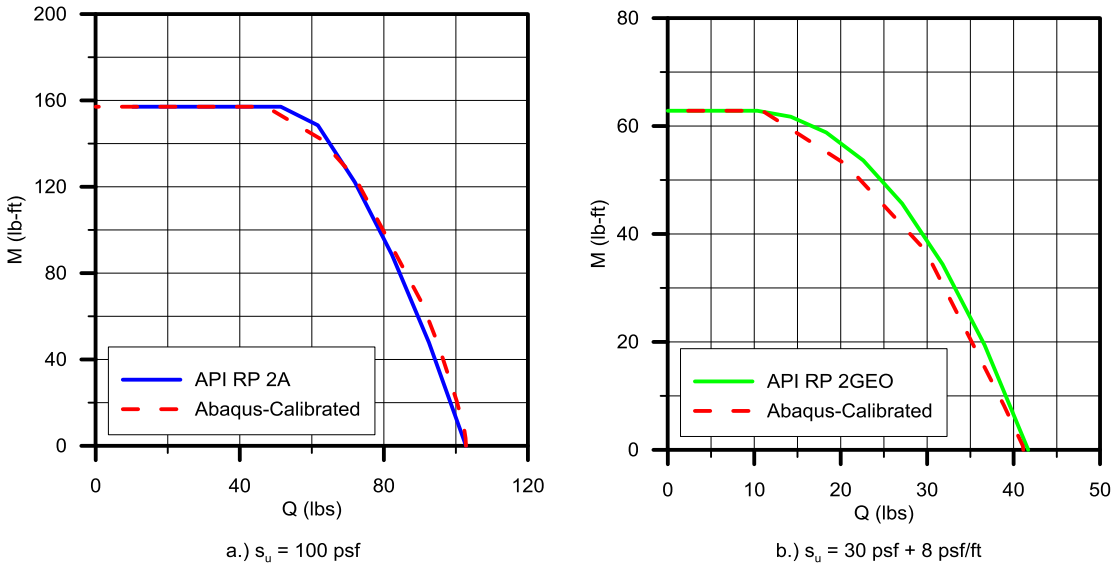

Figure 38. Comparison of results with calibrated ABAQUS results

Figure 39 plots the ultimate bearing capacity computed for each eccentric load applied to the foundation as calculated by:

- Upper bound plasticity analysis
- Calibrated ABAQUS results

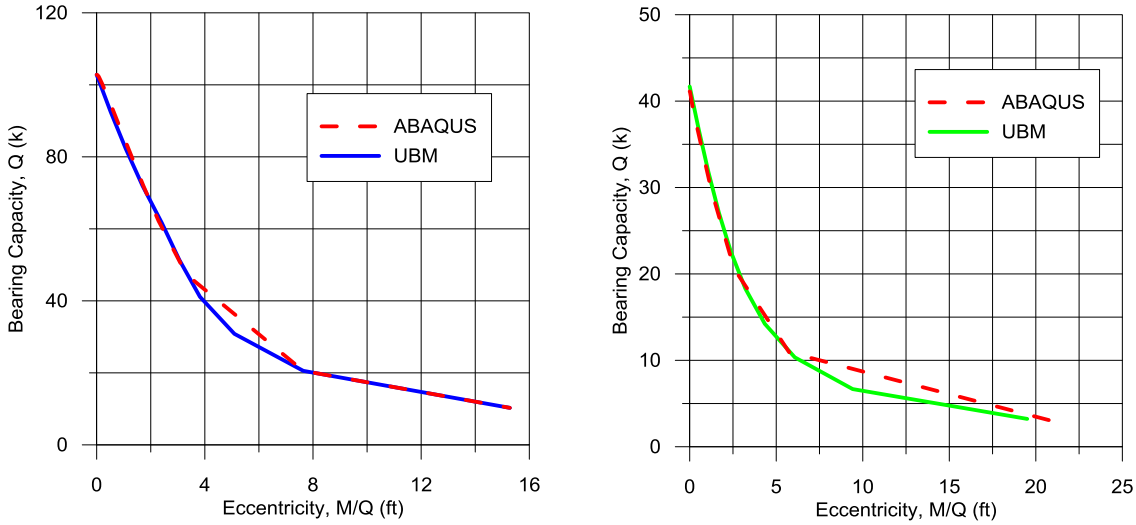

Figure 39. Eccentricity versus bearing capacity for UBM and ABAQUS results

It is shown in Figure 39 that for a given eccentricity, the calculated bearing capacities are similar in magnitude for the upper bound and ABAQUS analyses.

POTENTIAL SHORTCOMINGS OF PROPOSED ANALYSIS

Careful consideration should be made when using the proposed analysis presented in this thesis for mudmat design.

The bearing and overturning capacities calculated by this method assume that eccentric loading acts predominately in one direction (2-D analysis). This method would need modification to be used for mudmats with dominant eccentric loads in both planar directions.

The bearing and overturning capacities calculated by the method also neglect the effects of torsion. Significant torsion (or rotation about the vertical axis of the mudmat) will decrease the bearing and overturning capacity of a mudmat foundation.

This analysis neglects end effects caused by the shape of the foundation and assumes the bearing capacity factor, N_c, is to be equal to $2+\pi$. Thus, if the actual shape of the mudmat foundation is closer to a rectangle or square, the bearing and overturning capacity may be slightly underestimated. This is shown in Figure 40, where the interaction diagram for the mudmat foundation with two footings is shown calculated using the bearing pressure assuming a strip footing and assuming a rectangular footing of the actual dimensions shown in Figure 6.

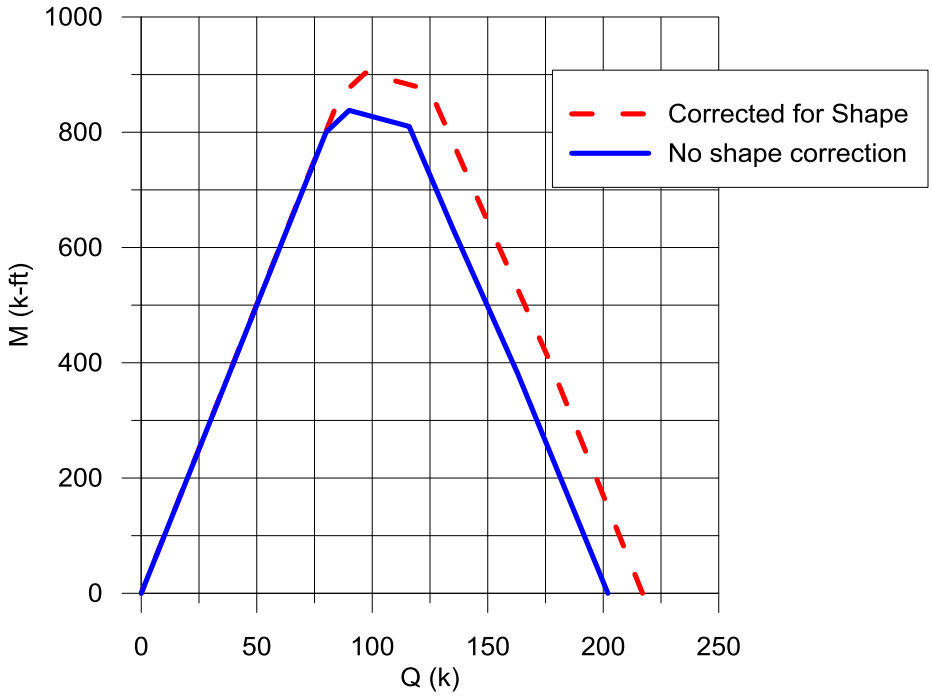

Figure 40. Interaction diagram for complex geometry with assumed end (shape) effect

CONCLUSIONS AND DISCUSSION

This thesis presents a simplified method for calculating the force-moment interaction relationship of a shallow foundation subject to eccentric loading. The method is particularly applicable to irregularly shaped foundations and composite foundations comprising multiple pods. The solution presented here applies an upper bound plasticity approach to the analysis of bearing and overturning capacity of shallow foundations. Validation is provided through FEM. This method is applied to challenges in offshore mudmat foundation design, although the principles are applicable to many other geotechnical analyses.

Key features of the method include:

1. The foundation is subdivided into one or more sub-elements according to the geometry of the footing. It is not necessary or desirable to subdivide a single rectangular section into sub-divisions.

2. A rotational failure mechanism entire is presumed, with the composite foundation assumed to act as a rigid body. The center of rotation can vary from zero (pure rotation) to infinity (pure vertical translation). The center of rotation is an optimization variable which will be varied to obtain a least upper bound.

3. The center of rotation for each sub-element is computed from kinematic considerations.

4. Equivalent bearing pressures acting on each component of the foundation are computed as a function of the center of rotation for that component. These equivalent pressures were established by matching to well-established solutions for pure vertical translation and pure rotation of a strip footing.

5. In cases of combined vertical-horizontal-moment (VHM) loading, a reduction in capacity due to the horizontal load is computed assuming a parabolic horizontal-vertical interaction function. Strictly speaking, the analysis does not adhere to an associated flow rule, since that would require that the work performed by the horizontal force be included in the energy balance. Future refinements to the analysis can strictly enforce an associated flow law.

6. Collapse load for a given center of rotation is computed by equating the external virtual performed by the applied load to the internal virtual work performed by the resisting soil.

7. The governing collapse load is taken as the lowest computed collapse load computed over a range of centers of rotation from zero to infinity.

We can conclude that the upper bound method provides a reasonable prediction of the bearing and overturning capacity of a mudmat foundation under eccentric loading. This conclusion is supported by the comparison of the magnitudes of the calibrated ABAQUS results with those from the upper bound method.

The results show that the force-moment interactions predicted by the upper bound method match well with the calibrated ABAQUS results, although the maximum overturning moments predicted by ABAQUS are slightly greater in magnitude. For design purposes, the lower magnitudes calculated by the upper bound method means more conservatism in the design than with FEM analysis.

The method presented here provides a simplified tool for routine calculations. In its present form, it is restricted to loads that are aligned with the major axes of the foundation. It presumes relatively simple soil strength profiles, uniform or linearly increasing with depth. More complex situations require more rigorous analyses, such as finite element or finite difference studies.

REFERENCES

American Petroleum Institute. (2010). Recommended Practice for Planning, Designing, and Constructing Fixed Offshore Platforms. *API RP 2A-WSD*.

American Petroleum Institute. (2011). Geotechnical and Foundation Design Considerations. *API RP 2GEO*.

Aubeny, C. P., & Murff, J. D. (2001). Lateral Undrained Resistance of Suction Caisson Anchors. *International Journal of Offshore and Polar Engineering, 11*, 211-219.

Calladine, C. R. (1969). *Engineering Plasticity.* Oxford: Pergamon Press.

Chen, W. F., & Liu, X. L. (1991). *Limit Analysis in Soil Mechanics.* New York: Elsevier Science Ltd.

Courant, R. (1942). Variational Methods for the Solution of Problems of Equilibrium and Vibrations. *Trans. American Mathematics Society, 1*, 1-23.

Davis, E. H., & Booker, J. R. (1973). The Effect of Increasing Strength with Depth on the Bearing Capacity of Clays. *Geotechnique, 23*, 551-563.

Drucker, D. C., & Prager, W. (1952). Soil Mechanics and Plastic Analysis for Limit Design. *Quarterly of Applied Mathematics, 7*, 157-165.

Gibson, R. E., & Morgenstern, N. R. (1962). A Note on the Stability of Cuttings in Normally Consolidated Clays. *Geotechnique, 12*, 212-216.

Gourvenec, S. (2007-1). Shape Effects on the Capacity of Rectangular Footings Under General Loading. *Geotechnique, 57*, 637-646.

Gourvenec, S. (2007-2). Failure Envelopes for Offshore Shallow Foundations under General Loadign. *Geotechnique, 57*, 715-728.

Gourvenec, S. (2008). Effect of Embedment on the Undrained Capacity of Shallow Foundations under General Loading. *Geotechnique, 58*, 177-185.

Gourvenec, S., & Randolph, M. (2003). Effect of Strength Non-Homogeneity on the Sahpe of Failure Envelopes for Combined Loading of Strip and Circular Foundations on Clay. *Geotechnique, 53*, 575-586.

Gupta, K. K., & Meek, J. L. (1996). A Brief Histroy of the Beginning of the Finite Element Method. *International Journal for Numerical Methods in Engineering, 36*, 3761-3774.

Han, S.-W. (2002). *The Capacity of Suction Caissons in Isotropic and Anisotropic Cohesive Soils Under General Loading.* Doctoral Dissertation. College Station: Texas A&M University.

Hansen, J. B. (1970). *A Revised and Extended Formula for Bearing Capacity.* Copenhagen: The Danish Geotechnical Institute.

Heyman, J. (1973). Simple Plasticity Theory Applied to Soil Mechanics. *Proceedings, Symposium on the Role of Plasticity Theory in Soil Mechanics*, (pp. 161-172). Cambridge.

Kim, B. M. (2005). *Upper Bound Analysis for Drag Anchors in Soft Clay*. Doctoral Dissertation. College Station: Texas A&M University.

Meyerhof, G. G. (1963). *Some Recent Research on the Bearing Capacity of Foundations*. Canadian Geotechnical Institute.

Murff, J. D. (2008). Notes for a Technical Short Course in Plastic Limit Analysis with Applications for Undrained Analysis of Foundations. Houston, TX.

Murff, J. D., & Aubeny, C. P. (2011). The effect of Torsion on the Sliding Resistance of Rectangular Foundations. *Proceedings, Frontiers in Offshore Geotechnics II*, (pp. 439-443). Perth, Australia.

Murff, J. D., & Hamilton, J. M. (1993). P-Ultimate for Undrained Analysis of Laterally Loaded Piles. *Journal of Geotechnical Engineering, 119*, 91-107.

Murff, J. D., & Miller, T. W. (1977-1). Foundation Stability on Nonhomogeneous Clays. *Journal of the Geotechnical Engineering Division, 103*, 1083-1095.

Murff, J. D., & Miller, T. W. (1977-2). Stability of Offshore Gravity Structure Foundations Using the Upper Bound Method. *Proceedings, Offshore Technology Conference*. Houston.

Murff, J. D., Wagner, D. A., & Randolph, M. F. (1989). Pipe Penetration in Cohesive Soil. *Geotechnique, 39*, 213-229.

Randolph, M. F., & Houlsby, G. T. (1984). The Limiting Pressure on a Circular Pile Loaded Laterally in Cohesive Soils. *Geotechnique, 34*, 613-623.

Randolph, M., Gaudin, C., Gourvenec, S., White, D., Boylan, N., & Cassidy, M. (2010). Recent Advances in Offshore Geotechnics for Deep Water Oil and Gas Developments. *Ocean Engineering, 10*, 818-834.

Sture, S. (2004). Finite Element Method in Geotechnical Engineering. Boulder, CO.

Vesic, A. S. (1975). Chapter 3 - Bearing Capcity of Shallow Foundations. In H. F. Winterkorn, & H. Y. Fang, *Foundation Engineering Handbook* (pp. 121-147). New York: Von Nostrand Reinhold Company.

Yun, G., & Bransby, F. (2007). The Horizontal-Moment Capacity of Embedded Foundations in Undrained Soil. *Canadian Geotechnical Journal, 44*, 409-424.

Yun, G., & Bransby, F. (2007). The Undrained Vertical Bearing Capacity of Skirted Foundations. *Soils and Foundations, 47*, 493-505.